



**HAL**  
open science

## Rock walls distribution and Holocene evolution in a mid-latitude mountain range (the Romanian Carpathians)

Mirela Vasile, Alfred Vespremeanu-Stroe, Daniela Pascal, Regis Braucher, Alin Pleșoianue, Răzva Popescu, Bernd Etzelmüller

### ► To cite this version:

Mirela Vasile, Alfred Vespremeanu-Stroe, Daniela Pascal, Regis Braucher, Alin Pleșoianue, et al.. Rock walls distribution and Holocene evolution in a mid-latitude mountain range (the Romanian Carpathians). *Geomorphology*, 2022, pp.108351. 10.1016/j.geomorph.2022.108351 . hal-03702052

**HAL Id: hal-03702052**

**<https://amu.hal.science/hal-03702052>**

Submitted on 22 Jun 2022

**HAL** is a multi-disciplinary open access archive for the deposit and dissemination of scientific research documents, whether they are published or not. The documents may come from teaching and research institutions in France or abroad, or from public or private research centers.

L'archive ouverte pluridisciplinaire **HAL**, est destinée au dépôt et à la diffusion de documents scientifiques de niveau recherche, publiés ou non, émanant des établissements d'enseignement et de recherche français ou étrangers, des laboratoires publics ou privés.

# Geomorphology

## Rock walls distribution and Holocene evolution in a mid-latitude mountain range (the Romanian Carpathians) --Manuscript Draft--

<b>Manuscript Number:</b>	GEOMOR-11671
<b>Article Type:</b>	Research Paper
<b>Keywords:</b>	rock wall morphometry; lithology; rock slope failures; Romanian Carpathians
<b>Abstract:</b>	<p>Rock walls in high mountain areas are the expression of long-term slopes response (10<sup>3</sup> –10<sup>5</sup> years) to tectonics, weathering and denudation and a major source of sediment and hazard. Mountain rock walls (RW) characteristics and evolution at mountain-range scale is rarely discussed in the literature. Using a database of 791 RW mapped in the Romanian Carpathians, we present their distribution and morphometry in respect to lithological class, structural features and topography and relate them to post-Younger Dryas (Holocene) rock slope failure chronology. Morphometric data indicate that metamorphic and igneous RW (linked to a great extent to glacial valleys and cirques headwalls) are usually restricted to the highest sectors of the mountain slopes, are characterized by reduced relative heights and have an asymmetrical distribution, being common on the North-exposed slopes but extremely rare on the South. Statistical analysis results show the high significance of structural and tectonic control on RW distribution in sedimentary units which imposes the predominance of West and North orientations and RW dimensions up to a degree higher than in other lithologies. Based on 38 10 Be surface exposure ages obtained on metric boulders from the Southern and Eastern Carpathians, we hypothesise that metamorphic and igneous RW in the formerly glaciated Carpathian valleys were significantly shaped during Early Holocene (before 9 ka) by rock slope failures events that followed the deglaciation of the highest cirques and the intense RW permafrost degradation. We associate the long-term imprints of frost weathering to the significant North/South RW and rock glaciers distribution asymmetry, also identified in other mid-latitude mountain sites with similar topographic constraints.</p>

Rock walls in high mountain areas are the expression of long-term slopes response ( $10^3$ – $10^5$  years) to tectonics, weathering and denudation and a major source of sediment and hazard. Mountain rock walls (RW) characteristics and evolution at mountain-range scale is rarely discussed in the literature. Using a database of 791 RW mapped in the Romanian Carpathians, we present their distribution and morphometry in respect to lithological class, structural features and topography and relate them to post-Younger Dryas (Holocene) rock slope failure chronology. Morphometric data indicate that metamorphic and igneous RW (linked to a great extent to glacial valleys and cirques headwalls) are usually restricted to the highest sectors of the mountain slopes, are characterized by reduced relative heights and have an asymmetrical distribution, being common on the North-exposed slopes but extremely rare on the South. Statistical analysis results show the high significance of structural and tectonic control on RW distribution in sedimentary units which imposes the predominance of West and North orientations and RW dimensions up to a degree higher than in other lithologies. Based on  $^{38} \text{Be}$  surface exposure ages obtained on metric boulders from the Southern and Eastern Carpathians, we hypothesise that metamorphic and igneous RW in the formerly glaciated Carpathian valleys were significantly shaped during Early Holocene (before 9 ka) by rock slope failures events that followed the deglaciation of the highest cirques and the intense RW permafrost degradation. We associate the long-term imprints of frost weathering to the significant North/South RW and rock glaciers distribution asymmetry, also identified in other mid-latitude mountain sites with similar topographic constraints.

1 **TITLE: Rock walls distribution and Holocene evolution in a mid-latitude**  
2 **mountain range (the Romanian Carpathians)**

3

4 Authors:

5 Mirela Vasile<sup>\*a</sup>, Alfred Vespremeanu-Stroe<sup>a,b</sup>, Daniela Pascal<sup>b,c</sup>, Regis Braucher<sup>d</sup>, Alin

6 Pleșoianu<sup>e</sup>, Răzvan Popescu<sup>a,b</sup>, Bernd Etzelmüller<sup>f</sup>

7

8 Affiliations:

9 <sup>a</sup> Research Institute of the University of Bucharest, 90-92 Sos. Panduri, 050663, sector 5, Bucharest,  
10 Romania

11 <sup>b</sup> Faculty of Geography, University of Bucharest, 1 N. Bălcescu Blv., 010041, sector 1, Bucharest,  
12 Romania

13 <sup>c</sup> Horia Hulubei National Institute for R&D in Physics and Nuclear Engineering, 30 Aleea Reactorului Str.,  
14 077125, Măgurele, Romania

15 <sup>d</sup> Aix-Marseille Univ., CEREGE, CNRS-IRD-Collège de France-INRAE BP 80, 13545 Aix-en-Provence  
16 Cedex 4, France

17 <sup>e</sup> ESRI Romania, 25 Washington Str., sector 1, Bucharest, Romania

18 <sup>f</sup> Department of Geosciences, University of Oslo, 1047, Blindern, Oslo, Norway

19

20 Corresponding Author:

21 Mirela Vasile, Research Institute of the University of Bucharest, 90-92 Sos. Panduri, 050663, sector 5,  
22 Bucharest, Romania, [mirela.vasile@geo.unibuc.ro](mailto:mirela.vasile@geo.unibuc.ro)

23

24 ABSTRACT

25 Rock walls in high mountain areas are the expression of long-term slopes response ( $10^3$ – $10^5$   
26 years) to tectonics, weathering and denudation and a major source of sediment and hazard.

27 Mountain rock walls (RW) characteristics and evolution at mountain–range scale is rarely  
28 discussed in the literature. Using a database of 791 RW mapped in the Romanian Carpathians,  
29 we present their distribution and morphometry in respect to lithological class, structural features  
30 and topography and relate them to post–Younger Dryas (Holocene) rock slope failure  
31 chronology. Morphometric data indicate that metamorphic and igneous RW (linked to a great  
32 extent to glacial valleys and cirques headwalls) are usually restricted to the highest sectors of  
33 the mountain slopes, are characterized by reduced relative heights and have an asymmetrical  
34 distribution, being common on the North-exposed slopes but extremely rare on the South.  
35 Statistical analysis results show the high significance of structural and tectonic control on RW  
36 distribution in sedimentary units which imposes the predominance of West and North  
37 orientations and RW dimensions up to a degree higher than in other lithologies. Based on 38  
38  $^{10}\text{Be}$  surface exposure ages obtained on metric boulders from the Southern and Eastern  
39 Carpathians, we hypothesise that metamorphic and igneous RW in the formerly glaciated  
40 Carpathian valleys were significantly shaped during Early Holocene (before 9 ka) by rock slope  
41 failures events that followed the deglaciation of the highest cirques and the intense RW  
42 permafrost degradation. We associate the long–term imprints of frost weathering to the  
43 significant North/South RW and rock glaciers distribution asymmetry, also identified in other  
44 mid-latitude mountain sites with similar topographic constraints.

45 KEYWORDS: rock wall morphometry; lithology; rock slope failures; Romanian Carpathians

46

## 47 1. INTRODUCTION

48 Mountain RW are landforms highly sensitive for mechanical weathering and erosional  
49 processes (Hales and Roering, 2007; Matsuoka, 2008; Allen and Huggel, 2013; Phillips *et al.*,  
50 2017), the rates of which are dictated by the interplay of lithology, climate and the local uplift  
51 regime (Willett 1999; Seong *et al.* 2009; Bartosch *et al.* 2017). Tectonics and structure  
52 significantly influence the extent and morphometry of the exposed rock surfaces in high

53 mountain areas (Lifton et al. 2009; Ellis and Barnes 2015; Sauchyn et al. 1998) which determine  
54 differential resistance to weathering and erosion. In formerly glaciated European mountain  
55 ranges, weathering and denudation rates are reported quantitatively after the Last Glacial period  
56 (Curry and Morris 2004; Hughes et al. 2007; Messenzehl et al. 2017; Matthews et al. 2018). The  
57 occurrence of numerous rock slope failures (RSF) in response to local deglaciation  
58 debuitressing has been documented by absolute age dating (Soldati et al., 2004; Prager *et al.*,  
59 2008; Ballantyne *et al.*, 2014) with responses varying from immediate to millennial time lags  
60 (Ballantyne *et al.*, 2014). The reconstruction of RSF chronology in Tatra Mountains (Pánek *et*  
61 *al.*, 2016) shows that lower magnitude events within steep topography occurred in the highest  
62 sectors of slopes hundreds of years after glacier retreat and are likely triggered by ice mass  
63 disappearance, whereas complex RSF producing at millennial time-scale in lower topography  
64 are associated with climate changing to warmer and more humid conditions during the onset of  
65 the Holocene and the Sub-Boreal period (Soldati et al., 2004; Ivy-Ochs *et al.*, 2009; Hermanns  
66 and Longva, 2013).

67 High-mountain rock slopes are a continuous source area for geomorphic processes that trigger  
68 natural hazards like debris flows, rockfalls or rock avalanches (Loye et al. 2009; Corona et al.  
69 2013; Kromer 2017), especially when affected by permafrost degradation. RW stability is  
70 responsive to climate variables such as changes of permafrost conditions (Krautblatter et al.  
71 2013; Girard et al. 2013) and global climate change influencing periglacial processes (Gruber et  
72 al., 2004; Messenzehl *et al.*, 2017; Phillips *et al.*, 2017), which has also been documented in  
73 warming conditions during the Holocene in the European and Scandinavian Alps (Hormes *et al.*,  
74 2008; Nagelisen *et al.*, 2015; Hilger *et al.*, 2021). This raises the question of RW evolution and  
75 subsequent debris production induced by the post-Younger Dryas permafrost retreat, especially  
76 in mid-latitude where permafrost in northerly slopes exists at lower altitudes than in southerly  
77 slopes (Magnin *et al.*, 2015).

78 Range-scale morphometric studies in the Romanian Carpathians have been documenting the  
79 distribution of glacial cirques by high-accuracy mapping (Mîndrescu and Evans 2014;  
80 Mîndrescu et al. 2010) and object oriented image analysis (Ardelean 2013). Geochronology  
81 studies based on absolute ages resume to deglaciation history, pointing to a Younger Dryas  
82 glacial advance at 12.9–12.1 ka only in the highest massifs (Popescu et al., 2017a). During the  
83 last decade, the intensive monitoring of the thermal regime of permafrost susceptible sites has  
84 shown the restrictive conditions for permafrost preservation in RW and rock glaciers  
85 (Vespremeanu–Stroe et al., 2012; Ardelean *et al.*, 2017; Onaca *et al.*, 2017; Popescu *et al.*,  
86 2017b). Recent studies on RW present state, in terms of stability or thermal regime,  
87 emphasized the rockfall hazard imposed by seasonal thawing in steep North-exposed RW  
88 (Vasile et al., 2014; Onaca *et al.*, 2015; Vasile and Vespremeanu–Stroe, 2017).

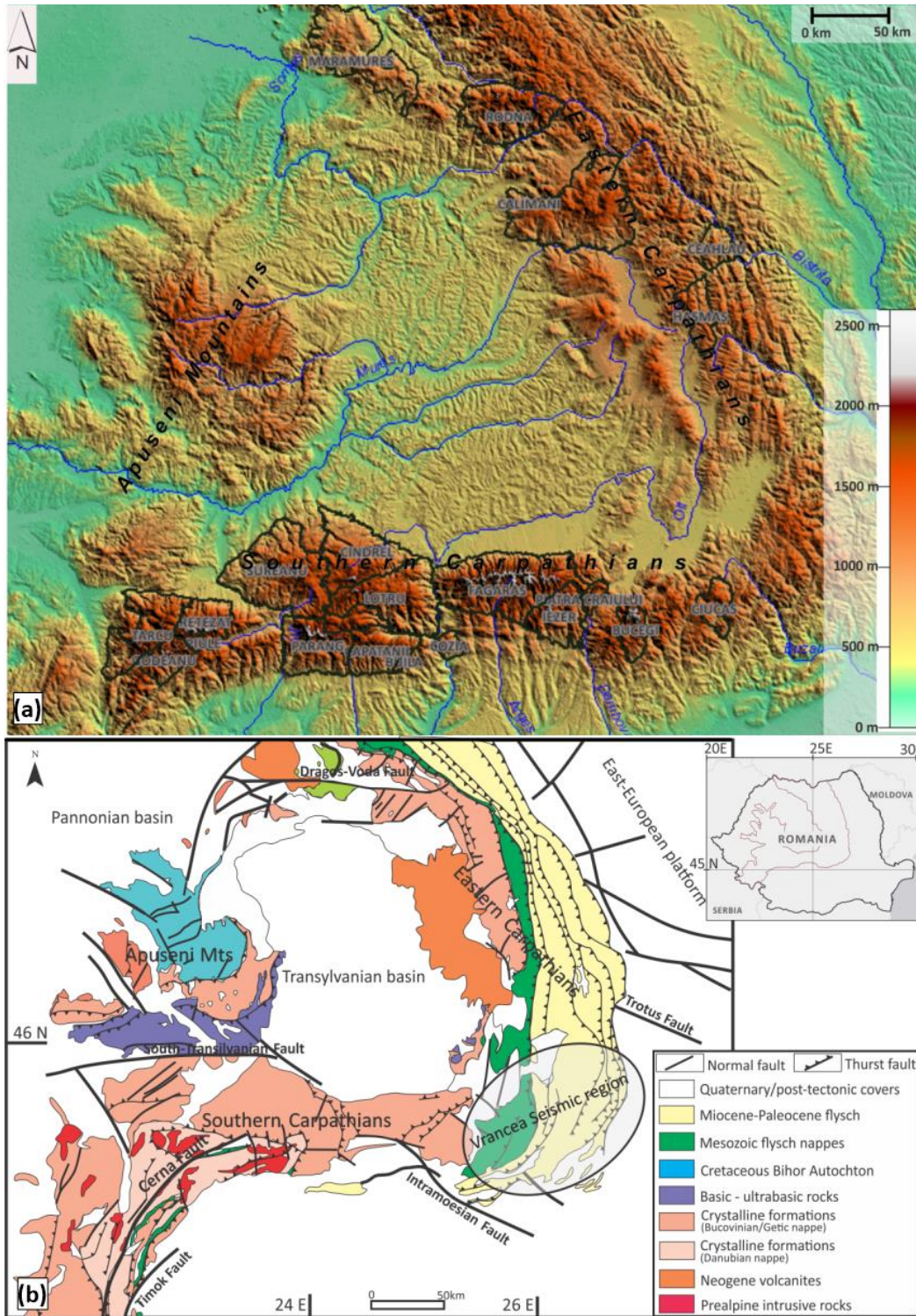
89 In this paper we i) present the distribution of RW in relation to lithology, structure and  
90 topography for assessing differential RW retreat control factors and ii) provide a first insight on  
91 Holocene RSF occurrence as the last major shaping agent of RW in the Romanian Carpathians.  
92 The objectives are achieved by RW mapping and statistical analysis of distribution controlling  
93 parameters, and by in-situ <sup>10</sup>Be surface exposure data analysis in glacial cirques and valleys  
94 from five different massifs.

95

## 96 **2. STUDY AREA**

97 The Romanian Carpathians stand as a geographical subdivision of the Carpathian Mountain Arc  
98 that stretches in Central and Eastern Europe (44° 30' – 47° 45' N and 21° 30' – 27° 10' E). They  
99 expand to a length of 900 km and reach the maximum altitude of 2544 m above sea level  
100 (a.s.l.). The three main subdivisions (i.e., the Eastern and Southern Carpathians – abbreviated  
101 EC and SC further on – and the Apuseni Mountains, Fig. 1a, b) show lithological and  
102 topographic differences that reflect the complexity of the geological evolution, structural  
103 characteristics, and influence of the Pleistocene glaciations.

104 The Carpathians are part of the Alpine Orogeny and include tectonic units dating prior to the  
105 alpine event, in the Palaeozoic and early Mesozoic. The youngest exhumation phases  
106 determined by thermochronology age patterns in the central part of the SC are Latest  
107 Cretaceous – Middle Eocene. The south–western sector of the SC underwent Oligocene –  
108 Miocene exhumation, whereas most of the EC correspond to Early – Middle Miocene phases,  
109 except for the SE Carpathians (Curvature Carpathians) which started uplifting in both Miocene  
110 and Latest Pliocene – Quaternary exhumation episodes (Merten, 2011). The EC are built on a  
111 central Crystalline Unit (correspondent to present Rodna, Maramureş, Rarău and Hăşmaş Mts.),  
112 Cretaceous Flysch (Ceahlău and Ciucaş Mts, extending towards the SC in Bucegi Mts) and  
113 Palaeogene Flysch (Table 1, Fig. 1b). Internal volcanism during the Miocene led to the  
114 formation of EC volcanic massifs while the Pliocene – Quaternary comprised both a rapid uplift  
115 of 500–1000 m (which led to the formation of the most recent depression areas), and the  
116 strongest volcanic activity in the area (Săndulescu, 1984; Linzer *et al.*, 1998; Mutihac, 2004).  
117 The SC are comprised of three major Crystalline Units: the Getic Overthrust Nappe (Şureanu,  
118 Căpăţanii, Lotru, Cindrel, Godeanu Mts), the Supragetic Overthrust Nappe (Făgăraş and Iezer  
119 Mts) and the Danubian Nappes (Retezat and Parâng Mts), the latter being formed by granitic  
120 and granodioritic batholiths in their central areas and marginal limestone massifs (Fig. 1a, b for  
121 location, Table 1).



122

123 **Figure 1:** (a) Location of Eastern and Southern Carpathians and Apuseni Mts., and outline of the units included in the  
 124 RW inventory (digital elevation by 1 arc-second resolution ASTER GDEM). (b) Simplified geological map of the  
 125 Carpathians (modified and adapted from Vaida and Verniers, 2005, and Merten, 2011. Small insert shows the  
 126 Carpathian Arc position in Romania (please refer to the colour version)

	Unit name (max. altitude)	Lithology/ Structure*	Extent / Direction	Nr. of mapped RW	Glaciation**
Eastern Carpathians	Maramureş (1956 m)	Crystalline schist with peripheral limestone and sandstones Volcanic intrusions (basalts)	15 km long / NW–SE ridge	11	Yes
	Rodna (2303 m)	Crystalline schist, micaschists and paragneiss Horst, Dragoş Vodă Fault	40 km long / E–W ridge	19	Yes
	Călimani (2100 m)	Andesites (volcanic) Eroded craters	Volcanic cone	5	Yes
	Ceahlău (1969 m)	Conglomerates and flysch Suspended syncline	15 km / N–S	10	No
	Hăşmaş (1973 m)	Massive limestone West oriented syncline	3.5 km long / NW–SE ridge	6	No
	Ciucaş (1954 m)	Conglomerates and sandstones, flysch East oriented syncline	Two separated ridges 7 km / SW–NE and 3 km / NW–SE	37	No
Southern Carpathians	Bucegi (2505 m)	Conglomerates, sandstones Limestone with radiolarites N–S syncline, East oriented cuesta front slope	Reversed U–shape 30 km long ridge	49	Yes
	Piatra Craiului (2238 m)	Limestone with radiolarites Hogback	25 km long / NNE–SSW ridge	13	No
	Iezer (2459 m)	Micaschists and paragneiss Supragetic overthrust nappe	20 km long / SW–NE ridge	27	Yes
	Făgăraş (2544 m)	Micaschists and paragneiss, amphibolite Supragetic overthrust nappe Northern–Făgăraş Fault Line	70km long W–E ridge, and multiple secondary N–S ridges	248	Yes
	Cozia (1668 m)	Gneiss Horst	~70 km <sup>2</sup> surface	3	No
	Buila–Vânturariţa (1885 m)	Massive Limestone Hogback	14 km long / SW–NE ridge	23	No
	Parâng (2519 m)	Granitoids Amphibolite (Danubian Unit)	25 km long / E–W ridge	40	Yes
	Şureanu/ Cindre/ Căpăţanii/ Lotrului (2130 – 2244 m)	Micaschists and paragneiss, amphibolite (Getic Unit)	15–25 km long / E–W ridges	8 / 10/ 4 / 5	Yes
	Retezat (2509 m)	Granodiorite intrusions Crystalline schist, amphibolite (Danubian Unit)	15 km long main / W–E ridge 2–5 km secondary N–S ridges	187	Yes
	Ţarcu (2196 m)	Conglomerates, sandstones, crystalline limestone Crystalline schist	20 km long / N–S then NE–SW ridge	26	Yes
	Godeanu/ Piule Iorgovanul (2291 m)	Micaschists and paragneiss, amphibolite / Recifal limestone	20 km long / NE–SW ridge	26 / 13	Yes
	Cerna Valley (1200 m)	Recifal limestone Graben	80 km long valley / NS	21	No

128 **Table 1:** Main lithological, structural and morphographic characteristics of the mountain units in which rock walls were  
129 mapped

130 \* according to the Geological Map of Romania, scale 1:200 000 (Geological Institute of Romania)

131 \*\* according to the Map of Glacial Cirques in the Romanian Carpathians (Mindrescu, 2016)

132 Present neo–tectonic movements show a differential uplift trend of the Carpathian orogeny with  
133 mean values of 1–3 mm/yr, higher values up to 3–5 mm/yr reported in the Eastern Făgăraş,  
134 Bucegi Mts. and the Curvature Carpathians which are associated with the activity from Vrancea  
135 seismic region (Hoeven *et al.*, 2005).

136 The past glacial activity in the Carpathian area is expressed by well-preserved glacial cirques,  
137 valleys and associated rock walls (Mîndrescu et al., 2010), most of which were modelled during  
138 LGM and Late Glacial cold phases (Popescu et al. 2017a).

139 The Romanian Carpathians are characterized by a temperate-continental climate, the mean  
140 annual air temperature (MAAT) ranging from -2°C at 2500 m a.s.l. (Vf. Omu meteorological  
141 station) and -0.4°C at 2190 m a.s.l. (Țarcu station) to 3 °C at 1577 m a.s.l. (Cozia station). Using  
142 a lapse rate of 0.63°C/100 m, the 0°C MAAT isotherm is around 2000 m a.s.l. on North-facing  
143 slopes and 2100 m a.s.l. on South-facing ones. Moisture is supplied by the West and SW  
144 dominating winds originating in the North-Atlantic and the Mediterranean, mean annual rainfall  
145 above 2000 m is 1100–1300 mm, snow cover reaches 1.5–2.0 m during January–March, and  
146 lasts in average 150–160 days per season (Micu *et al.*, 2015). In-situ RW thermal monitoring  
147 above 2200 m a.s.l. (Vasile and Vespremeanu-Stroe, 2017) exhibits prolonged seasonal frost  
148 (140–150 days/season with potential frost penetration depths reaching 2 m), and mean annual  
149 rock temperatures (MART) of 0.5°C on the North-exposed slopes and 3–4°C higher MART on  
150 the southern slopes, where daily temperature oscillations prevail, and continuous freezing rarely  
151 sets within the -3...-8°C freezing window.

152

### 153 **3. METHODS AND DATA**

#### 154 **3.1 Rock wall mapping**

155 RW were mapped based on the available time records of Google Earth satellite imagery.  
156 Because some images were not clear enough for a good differentiation between the RW and  
157 the adjacent geomorphological units, a comparison with higher resolution air photography was  
158 undertaken (orthophoto images available for view only from the National Agency for Cadastre  
159 and Land Legislation – ANCPPI at 1–5 m resolution). Further, the 25 m resolution EU-DEM  
160 digital surface model (EEA) was used to check slopes inclination and the inflection points within  
161 longitudinal profiles at the contact with the talus or at the top of the glacial cirques. The term

162 rock wall refers herein to steep, bare and compact rock surfaces, with angles usually higher  
163 than 37–40 degrees (Gruber, 2007). We took into account RW with areas larger than 200 m<sup>2</sup> in  
164 order to avoid patchy rock surfaces partially covered with vegetation or sporadic discontinuous  
165 outcrops. Considering these constraints, the analysis resumes to 21 mountain units in the EC  
166 and the SC (Fig. 1a for location), where rock surfaces matching these criteria were identified on  
167 satellite imagery. The geological map of Romania (scale 1: 200 000, Geological Institute of  
168 Romania) was used to determine the rock type of each mapped RW, assuring a complete  
169 spatial coverage over the entire range.

### 170 **3.2 Rock wall morphometry**

171 Mean RW area, total coverage, altitude, relative height, orientation and slope values were  
172 computed for each mountain unit (Table 2) and per lithology types, using the values from all  
173 units developed on the same rock class (sedimentary, igneous, metamorphic or volcanic). Each  
174 RW was vectorized and the resulting polygons were overlaid on the DEMs and then used for  
175 calculating the morphometric parameters in ArcGIS software. Mean RW orientation was  
176 determined by averaging raster direction. The RW area was calculated for a 2D projection of the  
177 RW polygons on the EU–DEM.

### 178 **3.3 Statistical analysis**

179 The statistical analysis was performed in RStudio (R version 3.4.0), and consisted in three  
180 stages. First, a data normality check was performed using the Shapiro–Wilk normality test  
181 (Shapiro and Wilk, 1965), which indicated the non-normality of the data. Then, for each  
182 mountain unit, a Kruskal–Wallis one–way analysis of variance test (Kruskal and Wallis, 1952)  
183 was performed in order to check if there are any statistically significant differences between  
184 groups of quantitative parameters, namely the relations between exposures and morphometry,  
185 and between lithology and morphometry. The Kruskal-Wallis Test is the non-parametric  
186 alternative to ANOVA (one-way analysis of variance), which checks if the analysed groups are

187 subsets from the same population. The test computes the rank variance of the interest variable  
188 for the combined groups, and then calculates the H statistic (Equation 1)

189 
$$H = \frac{N-1(gn_n(t_i-T_j)^2)}{gsn_n(t_j-T_i)^2},$$
 Equation (1)

190 where  $n_n$  is the sample size of the group,  $g$  is the sum of the group  $n$ ,  $sn_n$  is the sum of the  
191 corresponding group  $n$ ,  $t_i$  is the average observed rank sums for the group,  $t_j$  is the observed  
192 rank for a value in the corresponding group, and  $T_i$  is the observed total average rank sums.  
193 (McKight and Najab, 2010). The computed H statistic then indicates whether the groups come  
194 from the same population by comparing it to a critical value, which for our analysis corresponds  
195 to a 95% confidence or a p-value < 0.05. For H values beyond the critical threshold the Kruskal-  
196 Wallis Test indicates strong differences between analysed groups. Finally a post-hoc Dunn's  
197 Test (Dunn, 1961) for multiple comparisons was performed in order to identify which mountain  
198 units have significantly different values of each pair of the analysed parameters.

### 199 **3.4 Surface exposure ages**

200 24 boulders (20 from Făgăraş and four from Bucegi Mts) were sampled for cosmogenic  $^{10}\text{Be}$   
201 exposure dating. The samples are part of an extensive study regarding deglaciation and RSF,  
202 which counts more than 120 rock surfaces (unpublished data). During sample processing, the  
203 abundance of post-Younger Dryas resulting ages raised questions about RSF triggering the  
204 detachment of such boulders, as documented in other European mountain ranges (synthesis of  
205 studies in Pánek *et al.*, 2016). The samples included in the present study were collected along  
206 7 glacial valleys in Făgăraş Mts and one valley in Bucegi Mts, ranging from 1205 to 2287 m  
207 a.s.l., on metric-size boulders from both valley/cirque centre and peripheral. Sample size varied  
208 from 2 to 3 cm thick and sampled rock surfaces were vegetation free. Additionally, we  
209 accounted other 14 post-Younger Dryas boulder ages documented in the literature in Rodna  
210 (Gheorghiu, 2012), Parâng (Gheorghiu *et al.*, 2015) and Retezat massifs (Reuther *et al.*, 2007;

211 Ruszkiczay-Rüdiger *et al.*, 2021) which were considered as outliers in studies regarding  
212 deglaciation chronology, raising the database to 38 values from 16 valleys/cirques.

213 Secondary, we aimed for absolute dating of a rock glacier (Doamnei RG) surface in Făgăraș  
214 Mts., where we sampled four boulders from the RG body on a longitudinal profile but also the  
215 source RW area above; for comparing a North/South RW exposure, the corresponding South–  
216 face of Doamnei RW was also sampled.

217 Dating procedure for Făgăraș and Bucegi samples is described below.

218 The sample purification followed the procedure of Merchel and Herpers, 1999. Samples were  
219 crushed and sieved to the 0.25 – 1 mm fraction. Magnetic separation was performed on all  
220 samples with a magnetic separator “Frantz LB-1”. The other minerals that are embedded in  
221 samples were eliminated with mixtures of HCl and H<sub>2</sub>SiF<sub>6</sub>. Then atmospheric <sup>10</sup>Be was  
222 eliminated by HF (48%) dissolutions. Before the total dissolution, 150 mg of a <sup>9</sup>Be carrier  
223 solution (concentration 3025 ± 9 μg/g; Merchel *et al.*, 2008) manufactured in-house from a  
224 phenakite crystal were added to the samples. The total dissolution of quartz was performed with  
225 HF 48% (3.6 mL per g of quartz and 30 mL in excess). The resulting solutions were evaporated  
226 until dryness and samples were recovered with hydrochloric acid. Subsequently samples were  
227 precipitated with ammonia before successive separations through an anion exchange column  
228 (Dowex 1X8) to remove iron and a cation exchange column (Dowex 50WX8), and to discard  
229 boron and recover Be (Merchel and Herpers, 1999). BeO targets were prepared by mixing  
230 Niobium powder with the BeO oxide for AMS measurements.

231 All samples were chemically performed at *Laboratoire National des Nucléides Cosmogéniques*  
232 (LN2C) at CEREGE (Aix en Provence, France) and targets of purified BeO were prepared for  
233 AMS measurement at *ASTER, the French National AMS Facility* (CEREGE, Aix en Provence).  
234 The measurements were calibrated against an In-House standard (STD11) Braucher *et al.*,  
235 2015 standard, using an assigned <sup>10</sup>Be/<sup>9</sup>Be ratio of (1.191) × 10<sup>-11</sup> (1.09%). Analytical

236 uncertainties (reported as 1σ) included for all samples. The <sup>10</sup>Be half-life of (1.387±0.01) × 10<sup>6</sup>  
 237 years (Chmeleff *et al.*, 2010) was used.  
 238 Production rates were scaled following Stone, 2000 with a sea level high latitude production rate  
 239 of 4.02±0.36 atoms/g SiO<sub>2</sub>/yr (Borchers *et al.*, 2016). Rock density of 2.5 g/cm<sup>3</sup> was used for all  
 240 samples. Topographic shielding was calculated using the CosmoCalc 2.2 Excel add-in of  
 241 Vermeesch, 2007. Air pressure used is 1013 mBar. There was no quantitative information on  
 242 the snow cover during the surface exposure duration, hence, no corrections for potential effects  
 243 of snow cover or denudation were applied to the ages. <sup>10</sup>Be exposure ages were calculated  
 244 following Equation (2) using muogenic contributions of Braucher *et al.*, 2011.

$$\begin{aligned}
 245 \quad N(x, \varepsilon, t) = & \frac{P_{sp} * \exp(-\frac{x}{Ln})(1 - \exp(-t(\frac{\varepsilon}{Ln} + \lambda))}{\frac{\varepsilon}{Ln} + \lambda} \\
 246 \quad & + \frac{P_{\mu slow} * \exp(-\frac{x}{L_{\mu slow}})(1 - \exp(-t(\frac{\varepsilon}{L_{\mu slow}} + \lambda))}{\frac{\varepsilon}{L_{\mu slow}} + \lambda} \\
 247 \quad & + \frac{P_{\mu fast} * \exp(-\frac{x}{L_{\mu fast}})(1 - \exp(-t(\frac{\varepsilon}{L_{\mu fast}} + \lambda))}{\frac{\varepsilon}{L_{\mu fast}} + \lambda}
 \end{aligned}$$

248 Equation (2)

249 where:

250 N (x, ε, t) is the nuclide concentration function of depth x (g/cm<sup>2</sup>), denudation rate ε (g/cm<sup>2</sup>/y)  
 251 and exposure time t(y). *P<sub>sp</sub>*, *P<sub>μslow</sub>*, *P<sub>μfast</sub>* and *L<sub>n</sub>*, *L<sub>μslow</sub>*, *L<sub>μfast</sub>* are the production rates and  
 252 attenuation lengths of neutrons, slow muons and fast muons, respectively. *L<sub>n</sub>*, *L<sub>μslow</sub>*, *L<sub>μfast</sub>*  
 253 values used are 160, 1500 and 4320 g/cm<sup>2</sup>, respectively Braucher *et al.*, 2003. λ is the  
 254 radioactive decay constant. *P<sub>μslow</sub>*, *P<sub>μfast</sub>* are based on Braucher *et al.*, 2011.

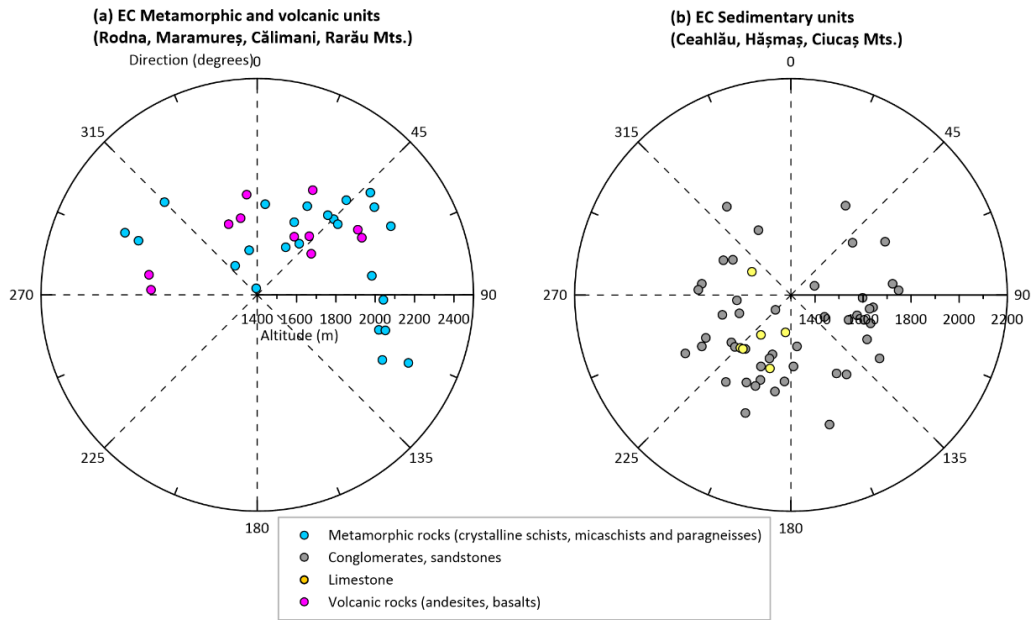
255

## 256 4. RESULTS

### 257 4.1 RW distribution

258 From the 21 units considered in this study, 11 preserve glacial landforms (Table 1). In the EC,  
259 only Rodnei, Maramureș, and Călimani massifs present visible glacial landforms (cirques,  
260 valleys and moraine deposits), most of which are in Rodnei Mts. (Mîndrescu 2016). The best  
261 preserved landforms are in Făgăraș Mts., where 207 glacial cirques were mapped (Mîndrescu  
262 et al. 2010), in Retezat Mts., which show extensive moraine deposits, glacial lakes and complex  
263 glacial valleys (Urdea, 2000), and in Parâng Mts., which keep the largest glacial cirques in the  
264 Romanian Carpathians (Iancu, 1970). The distribution of glacial cirques in the SC particularly  
265 reflects the main ridge orientation, with moderate differences of frequencies between North and  
266 South–exposed cirques (17% on North and 11% on South respectively, reported to 45 degrees  
267 bins) and the most favourable conditions of cirque glaciers formation on the East–exposed  
268 slopes of the valleys (19.5%) due to the strong eastward aeolian snow-transport acting on the  
269 crests and plateaus (Vespremeanu-Stroe et al., 2012). In terms of area and height, the North  
270 exposures preserve generally larger and wider cirques (Mîndrescu 2016).

271 A total of 791 RW were identified and considered as individual features, most of which were  
272 mapped in the SC. In most of the mountain units considered here, the main ridges follow East–  
273 West or NE–SW direction (Table 1), tracking the principal fault lines (Fig. 1a, b). The distribution  
274 of the RW is further presented, based on mean orientation and RW altitude.



275  
 276 **Figure 2:** Direction and mean altitude of the RW mapped in the EC: (a) the metamorphic schists – prevailing units;  
 277 the andesitic and basaltic outcrops are represented as volcanic RW; (b) the sedimentary units (limestone and  
 278 conglomerates prevailing). The radius of the graphs represents the altitude values, the general direction is expressed  
 279 in sexagesimal degrees and each dot represents a RW (please refer to the colour version)

280 The units from the EC count 88 mapped RW in total. The RW found in the schist–prevailing  
 281 massifs are distributed mainly on NE (23%) and secondary on North and East (Fig. 2a) with an  
 282 average altitude of 1950 m a.s.l., the North–exposed ones being situated at slightly lower  
 283 altitudes. The andesitic and basaltic rock outcrops mapped in the EC, are largely grouped on  
 284 the North and NE (82%) similarly with the metamorphic ones.

285 In the sedimentary units, RW extend on all orientations, with a maximum frequency on the  
 286 South (almost 40%) whilst just a few (7%) were mapped on the northern slopes (Fig. 2b), but  
 287 are limited to altitudes lower than 1800 m, reaching an average of 1634 m a.s.l. which is  
 288 considerably lower (> 300 m) than the metamorphic and volcanic RW.

289 Compared to the EC, the number of RW mapped in the mountain units from the SC built on  
 290 metamorphic rocks is much larger, rising to 331 from which 275 are distributed in two large  
 291 massifs (Făgăraș and Iezer), and the remaining are spread in 6 units characterized by gentler  
 292 topography and lower altitude (Fig. 3a, Table 2). The northern direction clearly dominates in

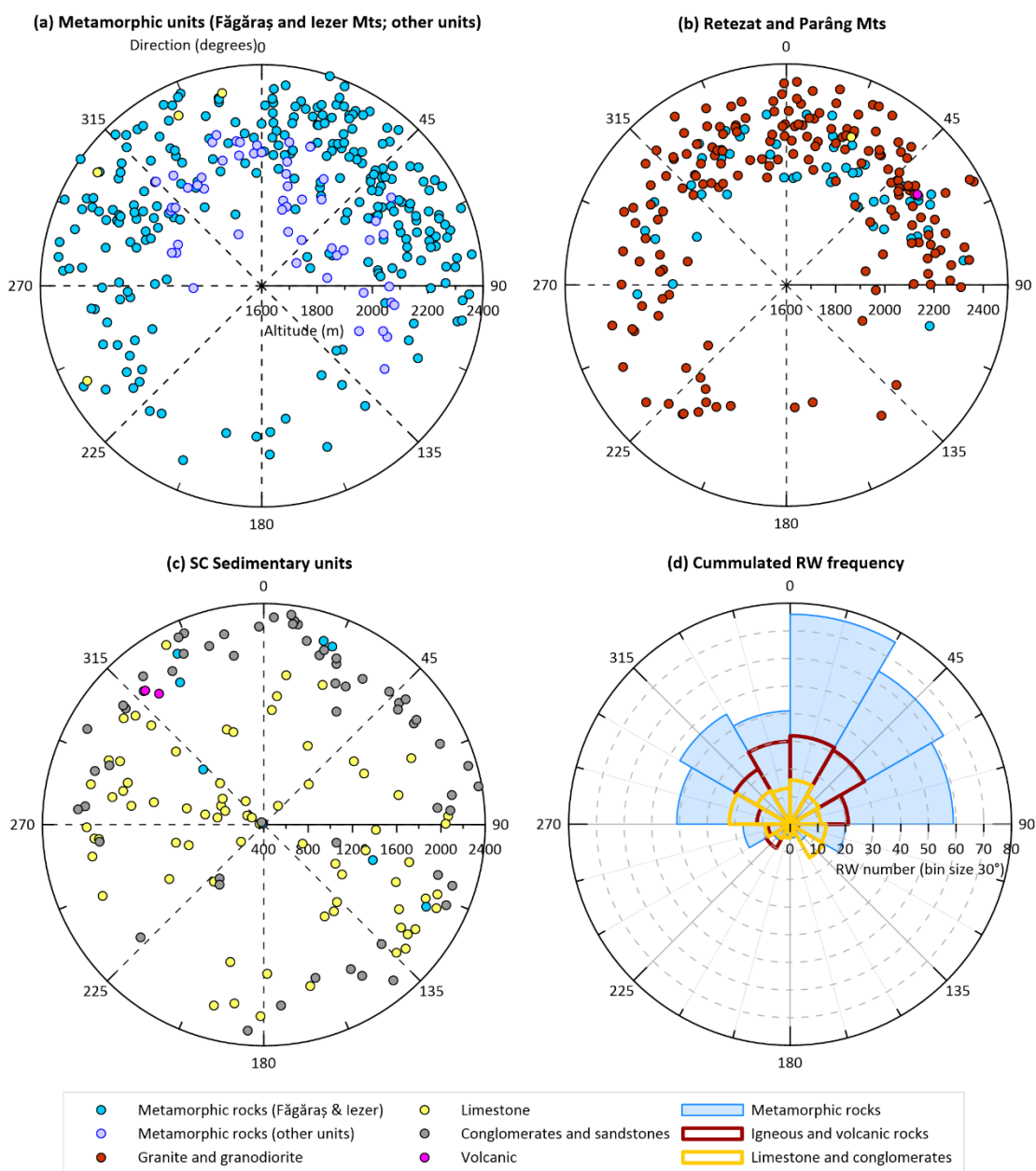
293 both clusters, summing 41% from the total RW number, with similar frequencies on the NW and  
 294 NE bins (Fig. 3d). The second highest RW frequency corresponds to the eastern orientation  
 295 (104 RW), followed by the western slopes (77 RW). RW mapped on the southern slopes are  
 296 scarce and represent 5.4% from the total number. In the large metamorphic massifs of Făgăraș  
 297 and Iezer the highest RW density is in the range of 2100 – 2400 m with a mean altitude of 2200  
 298 m (Table 2), but 14 mapped surfaces are higher than 2400 m.

	Units	Main Rock Types	RW count	Mean Area (m <sup>2</sup> x10 <sup>3</sup> )	Total Area (m <sup>2</sup> x10 <sup>3</sup> )	Mean Height (m)	Mean Slope (degrees)	Mean Alt (m)
Eastern C.	Călimani	Volcanic	5	4.79	23.97	35.8	39	1984
	Ceahlău / Hășmaș / Ciucaș	Limestone	6	59.45	356.71	162.5	44	1546
		Conglomerate	47	41.82	1965.95	83.5	35	1645
	Maramureș / Rodna	Schist	24	15.81	379.55	55.4	44	1950
		Volcanic	6	7.60	45.63	69.7	38	1799
	Bucegi	Conglomerate	42	116.16	4878.94	221.1	46	2096
		Limestone	7	72.5	507.51	175.5	48	1935
	Piatra Craiului	Limestone	13	220.82	2870.74	266.5	44	1967
	Făgăraș / Iezer	Schist	275	8.0	2200.78	73.1	41	2200
	Parâng / Retezat	Granite	175	12.5	2162.87	68.0	38	2229
Schist		52	22.94	1193.22	95.7	40	2169	
Southern C.	Buila / Piule-Iorgovanul / Țarcu / Cerna Valley	Limestone	70	34.1	1909.46	124.2	46	1346
		Conglomerate	17	14.38	244.47	59.3	41	1748
	Cozia / Cindrel / Șureanu / Lotrului / Căpățanii / Godeanu	Schist	8	8.75	70.04	65.3	46	1666
		Volcanic	2	4.83	9.67	46.0	39	1967
			Schist	56	4.61	258.25	33.0	38

299 **Table 2:** The averaged values of the morphometric parameters and total cumulated area of the mapped RW in EC  
 300 and SC

301 Parâng and Retezat Mts. in the SC (Fig. 1 for location) are two examples of mixed lithology,  
 302 being composed mainly of granitoids plus granodiorites intrusions and of crystalline schist,  
 303 micaschist, amphibolite (around 23% of the mapped surfaces) (Tables 1, 2) (Fig. 3b).  
 304 Approximately 54% of the RW from Parâng and Retezat Mts. are North-oriented. Eastern and  
 305 western exposures account for 25% and 15% of the total number, and only 5.7% of the mapped  
 306 surfaces from the two massifs were identified on the southern slopes. More than half of the RW  
 307 are concentrated in the 2100 – 2300 m interval and almost 18% extend above 2300 m, the  
 308 northern ones reaching the highest altitudes. The RW on metamorphic rocks in the two massifs

309 range at slightly lower altitudes and occur almost evenly on the East, North and West-oriented  
 310 slopes.



311

312 **Figure 3:** Direction and mean altitude of the RW mapped in the SC: (a) Făgăraș and Iezer Mts., with the secondary  
 313 cluster of RW mapped in the lower altitude SC metamorphic units; (b) distribution of igneous and metamorphic rock  
 314 surfaces in Parâng and Retezat Mts.; (c) distribution of limestone, conglomerate and sandstone RW mapped in SC;  
 315 (d) Cumulated RW distribution on the four main rock categories represented on 30 degrees direction bins (please  
 316 refer to the colour version)

317 In the limestone–prevailing units from the SC, (Bădescu and Tîrlă, 2020; see Fig. 1 for location),  
 318 69 RW were mapped (Fig. 3c), of which almost 40% are exposed towards West directions, 26%  
 319 to the East, 23% are on northern slopes, and 11% on the southern ones (Fig. 3d). In terms of  
 320 altitudinal distribution, there are also major discrepancies between the massifs, imposed by the  
 321 structural characteristics of each (Table 1). The highest mean altitude is recorded in Piatra  
 322 Craiului (1970 m) while Cerna Valley reaches the lowest (771 m).  
 323 Bucegi is the highest sedimentary massif (2507 m) from Carpathians, with most RW developed  
 324 on conglomerates and sandstones, and 15% on limestone outcrops. RW are distributed mainly  
 325 on the northern slopes (37%) and only 16% are South–facing. Maximum RW density is between  
 326 2100 and 2300 m for the North and East–exposed slopes. East, South and West RW are  
 327 situated at lower elevations and occur on a wider altitudinal range (1800 – 2200 m).  
 328 The statistical analysis shows the clear dominance of West–exposed RWs for most of the  
 329 considered morphometric parameters compared to the other main orientations (Table 3). This  
 330 asymmetry is however case–specific and imposed by the particular orientation of many of the  
 331 sedimentary units, respectively the NNE–SSW–oriented ridges and plateaus of Piatra Craiului  
 332 and Buila hogbacks, Bucegi, Ciucaș and Hășmaș synclines (Mutihac, 1990) or Cerna Valley  
 333 half–graben (Povară *et al.*, 2013), which together with the eastward and southward dipping  
 334 strata contribute to the larger occurrence of West and North–exposed RWs (Fig. 1b).

Ratio	Mean area	Height	Altitude
N/E	2.38 (**)	2.36 (**)	3.19 (***)
S/E	1.11 (·)	1.33 (·)	-3.7 (***)
W/E	5.34 (***)	5.71 (***)	-2 (*)
S/N	-0.41 (·)	-0.17 (·)	-6.05 (***)
W/N	3.66 (***)	4.1 (***)	-5.27 (***)
W/S	2.76 (**)	2.83 (**)	2.18 (*)

335 **Table 3:** Results of the statistical analysis (Post–Hoc Dunn’s Test) of morphometric parameters for pairs of main  
 336 exposures. Numbers represent the z-Score, which indicates whether the tested parameter pair has a value above the  
 337 rank mean (positive value), or below (negative value). For example, the mean area of N/E pair has a z-Score = 2.38,  
 338 meaning that North has a greater mean area than East. In a similar way, for z-Scores below the rank mean the

339 comparison is read inversely, as in the altitude for S/N pair which has a z-Score = -6.05, meaning that North has a  
 340 higher altitude than South  
 341 \* p-value (0.05, 0.01]; \*\* p-value (0.01, 0.001]; \*\*\* p-value < 0.001. A p-value < 0.05 indicates a strong statistical  
 342 significance at 95% confidence level

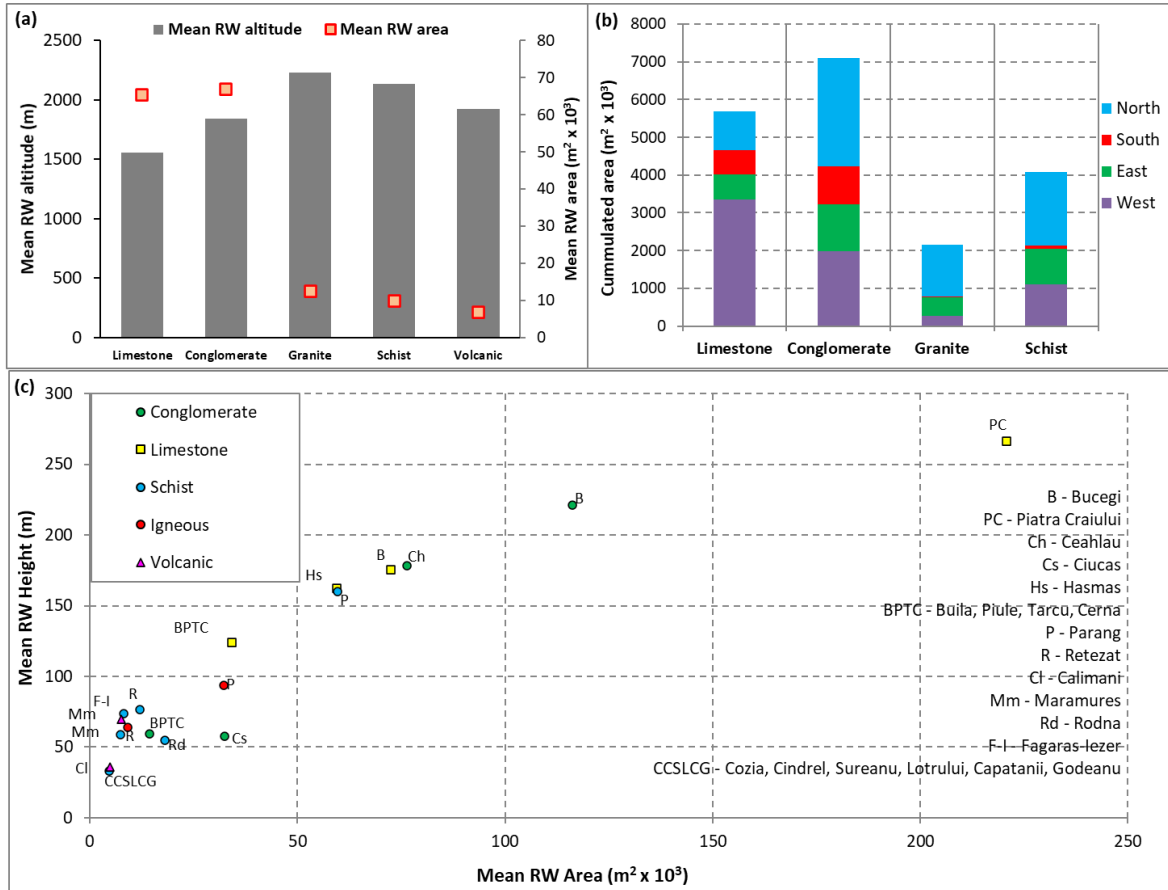
Ratio	Area	Height	Altitude
<b>Conglomerate/ Limestone</b>	-1.78 (*)	-3.9 (***)	2.93 (**)
<b>Granite/ Limestone</b>	-7.54 (***)	-6.9 (***)	12.89 (***)
<b>Schist/ Limestone</b>	-9.01 (***)	-8.36 (***)	10.9 (***)
<b>Granite/ Conglomerate</b>	-5.99 (***)	-2.79 (**)	10.31 (***)
<b>Schist/ Conglomerate</b>	-7.46 (***)	-3.87 (***)	7.91 (***)
<b>Schist/ Granite</b>	-0.77 (-)	-0.83 (-)	-4.53 (***)

343 **Table 4:** Results of the statistical analysis (Post-Hoc Dunn's Test) of morphometric parameters for pairs of main  
 344 exposures. Numbers represent the z-Score, which indicates whether the tested parameter pair has a value above the  
 345 rank mean (positive value), or below (negative value)  
 346 \* p-value (0.05, 0.01]; \*\* p-value (0.01, 0.001]; \*\*\* p-value < 0.001. A p-value < 0.05 indicates a strong statistical  
 347 significance at 95% confidence level

348 In summary, our observations indicate that RW in metamorphic and igneous units are generally  
 349 restricted to altitudes higher than 2100 m, show a high density on the North-exposed slopes  
 350 and lack from the southern ones. In comparison, RW distribution in sedimentary units is spread  
 351 over a larger range of altitudes but highly dependent on the structure and strata dip-direction  
 352 which result in prevalent West and North exposures but not as large (asymmetric) as for the  
 353 metamorphic and igneous rocks.

#### 354 **4.2 RW morphometry**

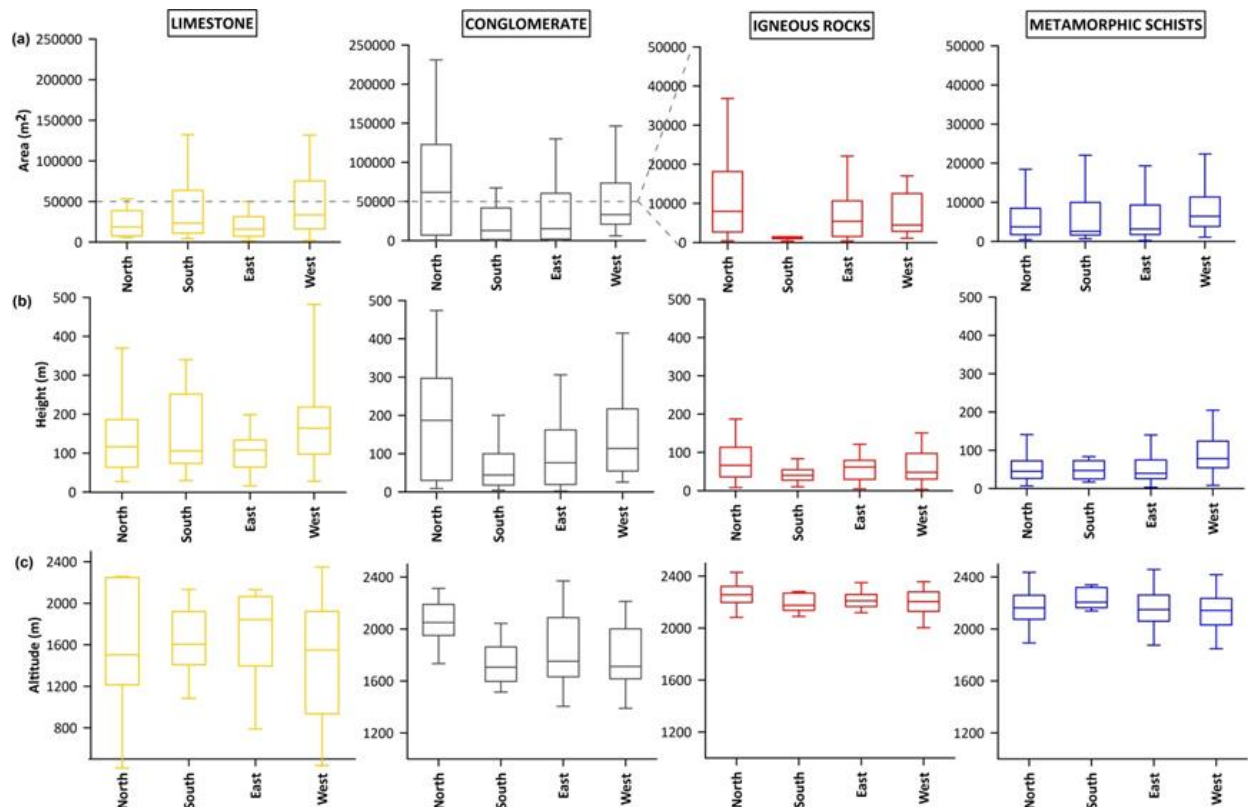
355 Although the most numerous RW were identified on metamorphic rocks, this group covers only  
 356 21% of the total mapped surface. An even smaller cumulated area corresponds to igneous  
 357 rocks which represent 12% of the total area. Comparatively, although counting less RW, the  
 358 sedimentary massifs cumulate 67% of the total mapped area due to their large mean surface  
 359 (Fig. 4a, b). Consequently, igneous and metamorphic RW are 5 to 6 times smaller than  
 360 limestone, conglomerates and sandstone RW (Fig. 5a).



361

362 **Figure 4:** General RW morphometry on the main rock types (counting all features corresponding to the same rock  
 363 type): (a) Mean RW altitude vs mean RW area; (b) Cumulated area of RW with the same lithology grouped on the  
 364 four main cardinal directions; (c) Mean RW height and area derived for each massif (please refer to the colour  
 365 version)

366 Metamorphic and igneous units are relatively similar in terms of RW vertical extension (around  
 367 70 m in average) and show little inter-site variation whereas the sedimentary units both for  
 368 limestone, conglomerate and sandstone RW reach almost double height values (Fig. 4c, 5b).  
 369 This visible heterogeneity is imposed by Bucegi and Piatra Craiului, with RW of up to 250 m  
 370 height. This is also consistent with the wider range of mean RW altitude, as limestone surfaces  
 371 extend at much lower altitudes (Fig. 5c).



372  
 373 **Figure 5:** Variability of the morphometry of the RW grouped in the main lithological classes in respect to the main  
 374 orientations: (a) mean RW area; (b) mean height; (c) mean altitude. The boxes display the median values, the 25–75  
 375 quartiles (lower – upper) and the caps show the minimum and maximum values (1.5 IQR)

376 Summing up, the high values of the z-scores in Table 4 (maximum -9.01 for schist/limestone  
 377 area, 10.9 for mean altitude) support the high morphometric differences that exist between the  
 378 sedimentary units and the metamorphic and igneous ones, which are more similar (-0.77 for  
 379 schist/granite area, -4.3 for altitude). Although more numerous, metamorphic and igneous RW  
 380 in the study area present typically small-size surfaces perched to the highest stands of formerly  
 381 glaciated valleys and cirques. The sedimentary (limestone and conglomerates prevailing) RW  
 382 are wider, steeper and cover larger areas than all the other lithological groups independent of  
 383 glacial landmarks and with apparent homogeneity in respect to slope orientation. These  
 384 characteristics thus reflect major differences between control factors over RW morphometry and  
 385 distribution depending on geology.

### 387 4.3 Absolute ages

388 Sample locations, altitudes,  $^{10}\text{Be}$  concentrations and  $^{10}\text{Be}$  surface exposure ages determined in  
389 this study and selected from the literature are presented in Table 5. Multiple values (3 to 5 per  
390 valley) available in 8 of the valleys presented here, allowed an intra and inter-massif analysis of  
391 age distributions. Values range between  $0.97 \pm 0.08$  ka and  $11.3 \pm 1.0$  ka (Table 5), clustering  
392 between 11.3 and 9.1 ka (21 values), thus immediately following the Younger Dryas (12.9–11.7  
393 ka, Rasmussen et al., 2006; 12.6–11.4 ka, Tămaş et al., 2005) and within time lags of up to 2.6  
394 ka after. A second high frequency cluster was found between 9.0 and 7.0 ka, while younger  
395 ages were identified with a frequency of 1.75 values/1000 yrs. There is not a clear correlation  
396 between the absolute ages of the rock surfaces and the altitude. Such an attempt would be  
397 hindered by the unequal sample distribution, given the fact that most of the boulders are  
398 situated above 1800 m a.s.l. Nevertheless, most of the youngest ages ( $0.94 \pm 0.08$  ka,  $4.51 \pm$   
399  $0.18$  ka,  $2.19 \pm 0.12$  ka,  $1.27 \pm 0.22$  ka) were found in the lower or mid-sectors of Dejani, Bâlea  
400 and Sâmbăta valleys (Făgăraş Mts.), between 1200 and 1500 m a.s.l., respectively. Although  
401 few ages from the onset of the Holocene were also determined below 1400 m in the Retezat  
402 and Parâng Mts., ( $10.7 \pm 1.4$  ka, Ruszkiczay-Rüdiger *et al.*, 2021,  $10.5 \pm 0.9$  ka, Gheorghiu *et*  
403 *al.*, 2015), most boulders dating between 11.5 and 7.0 ka are situated in the highest sector of  
404 the valleys and on cirque floors (1800–2200 m a.s.l.). This distribution pattern is similar when  
405 comparing both valleys within the same massif (e.g., Făgăraş) and valleys from the five different  
406 massifs (Table 5).

407 The samples from Doamnei rock glacier yielded values of  $12.97 \pm 0.38$  and  $11.44 \pm 0.34$  ka in  
408 the front sector, which gradually decrease to  $9.91 \pm 0.45$  in the middle part and  $3.37 \pm 0.10$  ka at  
409 RW base. The exposure date of the source RW and the youngest rock glacier boulder age from  
410 the upmost sector indicate rockfalls activity during Late Holocene (Table 5). Comparatively, the  
411 South-exposed side of the ridge has returned a much older age ( $52.64 \pm 0.89$  ka).

412

LOCATION	Sample name	Lat	Long	Altitude (m)	Quartz mass (g)	[ <sup>10</sup> Be] atoms g <sup>-1</sup> x 10 <sup>4</sup>	t (exposure time) ka	Source
<b>FĂGĂRAȘ</b>								
Arpaș	AR01	45.60	24.67	2134	23.23	8.76 ± 0.33	4.07 ± 0.13	this study <sup>a</sup>
Bâlea Valley	BL	45.64	24.60	1205	24.39	4.92 ± 0.18	4.51 ± 0.18	
Dejani Valley	DEJ01	45.61	24.94	1300	23.05	1.13 ± 0.10	0.97 ± 0.08	
Dejani Valley	DEJ02	45.61	24.94	1287	26.72	8.15 ± 0.31	7.11 ± 0.26	
Dejani Valley	DEJ03	45.59	24.94	1929	26.00	16.91 ± 0.63	9.11 ± 0.34	
Dejani Valley	DEJ04	45.60	24.94	1401	25.77	13.36 ± 0.50	10.55 ± 0.39	
Fundul Caprei Valley	FC02A	45.60	24.64	1850	23.11	15.71 ± 0.59	9.04 ± 0.33	
Mioarele cirque	MIO01	45.58	24.83	2287	26.41	24.28 ± 0.91	10.14 ± 0.38	
Mioarele cirque	MIO02	45.58	24.83	2274	22.88	24.18 ± 0.76	10.14 ± 0.31	
Mioarele	MIO03	45.58	24.83	2285	24.74	24.33 ± 0.91	10.15 ± 0.38	
Orzâneaua cirque	ORZ02	45.60	24.72	1985	25.55	16.98 ± 0.64	8.79 ± 0.33	
Sâmbăta Valley	VS02	45.61	24.80	1823	25.11	16.60 ± 0.62	9.65 ± 0.36	
Sâmbăta Valley	VS01	45.61	24.80	1796	23.66	16.77 ± 0.57	9.95 ± 0.33	
Sâmbăta Valley	SA07	45.64	24.79	1215	26.22	2.46 ± 0.09	2.19 ± 0.12	
Sâmbăta Valley	SA05	45.62	24.79	1485	14.56	1.87 ± 0.07	1.27 ± 0.22	
Sâmbăta Valley	SA04	45.36	24.47	1820	-	-	10.00 ± 0.30	
Urlea cirque	U04	45.60	24.84	2077	25.44	16.00 ± 0.60	7.92 ± 0.29	
Urlea cirque	U01	45.60	24.84	2134	22.88	19.68 ± 0.59	9.36 ± 0.28	
Urlea cirque	U06	45.60	24.85	2062	27.87	22.14 ± 0.83	10.86 ± 0.40	
Urlea cirque	U01A	45.60	24.84	2130	23.07	22.94 ± 0.86	10.95 ± 0.41	
Doamnei RW N	DBEN	45.35	24.36	2230	20.48	3.59 ± 0.24	2.07 ± 0.13	
Doamnei RW S	DBES	45.35	24.36	2243	20.24	121.18 ± 2.06	52.46 ± 0.89	
Doamnei RG1	DBE1	45.36	24.36	2057	20.33	20.39 ± 0.94	9.91 ± 0.45	
Doamnei RG2	DBE2	45.36	24.36	2062	20.61	26.71 ± 0.79	12.97 ± 0.38	
Doamnei RG3	DBE3	45.36	24.36	2082	21.07	23.88 ± 0.71	11.44 ± 0.34	
Doamnei RG4	DBE4	45.35	24.36	2133	20.70	7.01 ± 0.22	3.37 ± 0.10	
<b>BUCEGI</b>								
Gaura Valley	Gaura05	45.43	25.40	1541	25.41	15.76 ± 0.61	10.78 ± 0.43	
Gaura Valley	Gaura06	45.43	25.40	1545	25.74	15.50 ± 0.46	10.62 ± 0.33	
Gaura cirque	Gaura03	45.44	25.43	2072	15.44	15.72 ± 0.49	7.49 ± 0.23	
Gaura cirque	Gaura01	45.44	25.43	2081	25.39	15.60 ± 0.53	8.00 ± 0.25	
<b>PARANG</b>								
lezer Valley	PR01	45.34	23.63	2034	10.99	24.34 ± 1.08	11.20 ± 0.50	Gheorghiu <i>et al.</i> (2015) <sup>b</sup>
lezer Valley	PR03	45.34	23.62	1970	14.33	13.61 ± 0.46	6.20 ± 0.20	
lezer Valley	PR05	45.34	23.62	2008	10.6	19.64 ± 0.63	8.80 ± 0.80	
Gâlcescu cirque	PR10	45.35	23.61	1990	8.21	24.29 ± 0.69	11.20 ± 0.30	
Zănoaga Mare cirque	PR15	45.35	23.59	2055	10.19	23.63 ± 0.70	10.20 ± 0.30	
Zănoaga Mare cirque	PR16	45.35	23.59	2055	10.56	23.94 ± 0.83	10.40 ± 0.30	

**Table 5:** Sampling locations, <sup>10</sup>Be concentrations, and <sup>10</sup>Be surface exposure ages for post–Younger Dryas dated boulders in the Romanian Carpathians

<sup>a</sup> Analytical uncertainties (reported as 1-σ) included for all samples. No corrections for potential effects of snow cover or denudation were applied to the ages

<sup>b</sup> Exposure ages calculated using Cronus-Earth 10Be - 26Al exposure age calculator v. 2.2 (<http://hess.ess.washington.edu/>). They assume zero erosion, scaling factors according to Stone (2000) and a spallation production rate of 4.49 ± 0.39 atom (g SiO<sub>2</sub>)<sup>-1</sup> a<sup>-1</sup> (Balco *et al.*, 2008). Exposure ages are presented with the external uncertainties

RETEZAT								
Lăpușnicu Valley	Re15-29	45.31	22.78	1167	-	10.30 ± 0.13	10.70 ± 1.40	Ruszkiczay-Rüdiger <i>et al.</i> , (2021) <sup>c</sup>
Pietrele Valley	Pt-03-02	45.28	22.88	1902	-	23.9	11.40 ± 1.30	Reuther <i>et al.</i> (2007) <sup>d</sup>
RODNA								
Pietroasă Valley	RD 30	47.61	24.64	1379	25.11	16.32 ± 0.50	10.50 ± 0.90	Gheorghiu, (2012) <sup>ee</sup>
Zănoaga Mare cirque	RD 04	47.6	24.64	1669	28.95	21.65 ± 0.63	11.50 ± 1.00	
Zănoaga Mare cirque	RD 06	47.6	27.63	1767	24.24	22.83 ± 0.63	11.30 ± 1.00	
Zănoaga Mare cirque	RD 07	47.6	27.63	1767	25.85	22.50 ± 0.65	11.10 ± 1.00	
Zănoaga Mare cirque	RD 05	47.6	27.63	1753	24.36	10.89 ± 0.40	5.70 ± 0.50	
Buhăiescu Valley	RD 19	47.58	24.65	1718	23.01	21.61 ± 0.63	10.40 ± 0.90	

<sup>c</sup> The measured  $^{10}\text{Be}/^{9}\text{Be}$  AMS ratios were corrected for full processed blank ratios:  $(3.30 \pm 0.50) \times 10^{-15}$ . Age uncertainties: the 1st number is the internal uncertainty (AMS measurement, weighting, carrier, blank and half-life;  $1-\sigma$ ). Every reported age was corrected for topographic- and self-shielding

<sup>d</sup> Exposure age corrected for the effect of topographic shielding and surface geometry

<sup>e</sup> Exposure ages calculated using Cronus-Earth  $^{10}\text{Be} - ^{26}\text{Al}$  exposure age calculator v. 2.2 (<http://hess.ess.washington.edu/>). They assume zero erosion, scaling factors according to Stone (2000)

## 413 5. DISCUSSION

### 414 5.1 Structure and lithology influence on RW distribution

415 The RW inventory and morphometric analysis results have emphasized the significant influence  
416 of the lithology and geological structure on the characteristics of metamorphic, igneous and  
417 sedimentary RW in the Romanian Carpathians, the first two rock categories producing much  
418 smaller RW, but developed at higher altitudes, than sedimentary massifs which account for the  
419 greatest rock surface coverage overall. Our results also showed that the distribution of RW in  
420 the Carpathians is very particular in respect to orientation, with an obvious asymmetry between  
421 North and South exposures especially for metamorphic and igneous rocks, yet with extent RW  
422 on all orientations in limestone or conglomerate massifs.

423 Despite the North / South balanced distribution of the glacial cirques (Mindrescu, 2016), we  
424 showed that RW present a high asymmetry in the metamorphic and igneous mountain units  
425 from the both SC and EC (Fig. 2a, 4b, d), where South-exposed slopes are much less frequent  
426 whilst the total covered area is almost 30 times higher on the North-exposed RW.

427 Correspondently, the present rock glaciers distribution in these units accounts for 58% of the  
428 mapped rock glaciers in the northern quadrant, and only 13% in the southern one (Onaca *et al.*,  
429 2017), which also suggests a more intense/frequent debris accumulation on the North exposed  
430 slopes during Younger Dryas and Early Holocene when presumably most of the rock glaciers  
431 formed (Onaca *et al.*, 2013). A similar distribution is described in the Adamello–Presanella  
432 massif (Italian Alps), where the main ridge follows the NE-SW direction of the North-bordering  
433 fault and valleys radiate from the main ridge, covering all the cardinal directions. Here, based on  
434 the inventory of 216 rock glaciers mostly consisting of intrusive granodioritic and tonalitic rocks,  
435 Baroni *et al.*, (2004) show that both active and relict rock glaciers are predominantly facing the  
436 North, NW and NE compared to the southern quadrant (which counts 18% of the active /  
437 inactive, and 15% of the relict ones), and argument, by comparing front altitudes, that local  
438 topoclimate makes northern slopes more favourable to rock glacier formation and preservation.  
439 We further consider that RW preservation conditions are also more restrictive on the southern  
440 slopes in igneous and metamorphic slopes, as commented below.

441 Both granite and schist RW in the study area are characterized by metric joints networks which  
442 fit well with the dimensions of the boulders enclosed into the adjacent debris deposits (Vasile  
443 and Vespremeanu-Stroe, 2017), supporting intense slope modelling which could have led to the  
444 formation of large debris deposits, talus cones and rock glaciers. In a simulation of moisture  
445 availability in alpine RWs, (Rode *et al.* 2016) highlight that the preconditions of water saturation  
446 and temperature required for ice segregation are often recorded on the North-exposed slopes  
447 but just rarely met on warmer South–exposed rock surfaces, which implies that the latter are not  
448 prone for large–size debris production. Thus, South–exposed rock slopes would be subject to  
449 small–scale flake and granular rock shattering under the effect of both superficial freezing  
450 during snow melting intervals (Matsuoka, 2008) and of diurnal insolation thermal stress during  
451 snow–free intervals (Eppes *et al.*, 2016). We assume that South–exposed RW in the Romanian  
452 Carpathians were generally more stable than the other exposures whilst the northern were the

453 most active due to longer permafrost preservation. This is also supported by the old age (52.46  
454  $\pm 0.89$  ka) age yielded by the South-exposed ridge outcrop above Doamnei rock glacier, which  
455 was apparently unaffected by LGM, when it most probably stood as nunatak. Humification  
456 process (i.e. humus formation in soil profiles) has been inferred to be more intense on South-  
457 exposed mountain slopes, where warmer conditions intensify oxidation and create a more  
458 optimal environment for microorganisms that degrade organic matter (Egli *et al.*, 2010),  
459 compared to North-exposed mountain slopes which incorporate undecomposed or weakly  
460 degraded organic matter and are subject to mineral leaching due to colder and wetter  
461 conditions. Savi *et al.* (2015) reconstruct frost-cracking intensity and debris production during  
462 the Holocene in the Eastern Italian Alps, and emphasizes that high debris accumulation  
463 occurred during Early Holocene and also during Atlantic and Subatlantic periods when positive  
464 MAAT would have promoted continuous superficial (up to 100 cm deep) frost cracking in the  
465 highest peaks (around 3000 m a.s.l.). A similar pattern is supported in the SC by the surface  
466 exposure ages that sustain production of large debris in all massifs during Early Holocene and  
467 secondary debris production in subsequent phases.

468 The cumulated effect of these processes could explain a generally faster cover with soil and  
469 vegetation on the sunny slopes of both metamorphic and igneous units from this study, whereas  
470 on the North, colder thermal regime and the production of large-size boulders led  
471 simultaneously to a better preservation of RW, which is reflected in present-day distribution and  
472 morphometry.

473 The large synclines represented by Bucegi and Ciucaș Mts., with main North to South dip  
474 direction of the conglomerate and sandstones bedding planes uplifted large RW on the North-  
475 facing cuesta fronts, typical for sedimentary units formed as synclines, perched synclines, or  
476 hogbacks which are generally dominated by the compactness and steepness of the cuesta  
477 escarpments (Huggett, 2007). This is also the case in the NE-SW-dipping limestone massifs in  
478 SC which enhanced the development of the largest RW on their western slopes. Limestone RW

479 in both EC and SC generally lack dense superficial joint networks which, along with increased  
480 permeability, limits water availability within the first centimetres of rock and implicitly turns ice  
481 segregation less probable, which implies reduced RW modelling by frost shattering and debris  
482 accumulation in sedimentary massifs (Johnson et al., 2007). This is reflected by the low number  
483 of rock glaciers formed / identified in the SC on sedimentary rocks (only 15 on limestone from a  
484 total statistical population of 306 rock glaciers; Onaca et al. 2017). Therefore, we consider the  
485 lithology and structure to play the major role in imposing the orientation-related homogeneity  
486 which accounts as the primary control in RW distribution and dimensions in the sedimentary  
487 units from this study. Secondary, post-glacial RW relaxation would have led to the detachment  
488 of massive limestone and conglomerate blocks as sustained by the absolute ages obtained in  
489 Bucegi Mts (Table 5). However, in specific cases, such as Piatra Craiului limestone hogback,  
490 large debris deposits have accumulated at the base of the main tectonic slopes. For such  
491 cases, we assume that the absence of transversal valleys and of the Pleistocene glaciers, both  
492 caused by topography, could have created the conditions for the long-term (e.g. Middle to Late  
493 Quaternary) debris accumulation, the formation of which is still to be deciphered.

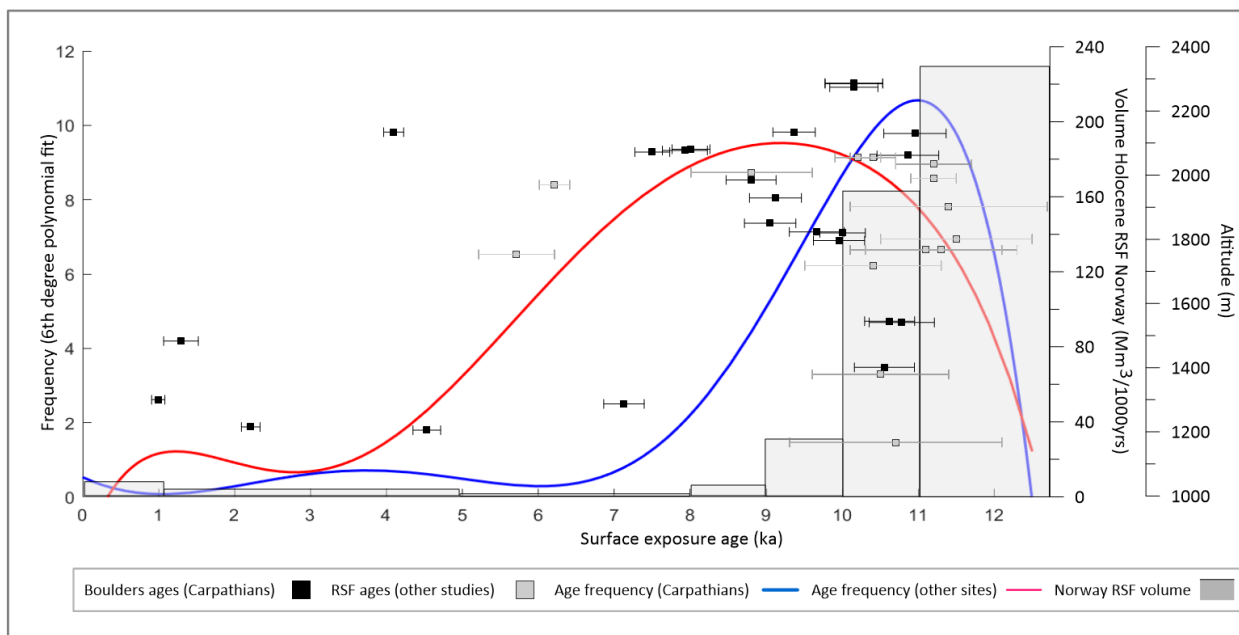
## 494 **5.2 Holocene dynamics of RW depicted by rock-slope failures**

495 Following Last Glacial Maximum deglaciation (19-14.5 ka), small glaciers re-occupied the  
496 highest cirques (> 2050 m) during Younger Dryas excepting the southern ones (Gheorghiu *et*  
497 *al.*, 2015; Popescu et al., 2017a; Pascal et al., 2018). The largest Younger Dryas glaciers are  
498 likely to have lasted more than a millennium during Early Holocene (e.g.  $10.2 \pm 0.9$  kyrs,  
499 Gheorghiu *et al.*, 2015). Therefore, we consider that most of the boulders from high altitudes (>  
500 2000 m) of early Holocene age dated in this study have originated by RW destabilization as  
501 response of ice retreat which occurred mainly in the upper valley/cirques sectors where glaciers  
502 were restricted (Fig. 6). High frequency of such events occurring several thousand years after  
503 Younger Dryas period are well documented in the European Alps (Soldati et al., 2004; Cossart  
504 *et al.*, 2008; Hormes *et al.*, 2008; Prager *et al.*, 2008; Ivy-Ochs *et al.*, 2009), Tatra Mts. (Pánek

505 *et al.*, 2016), in Scotland (Ballantyne *et al.*, 2014) and Scandinavia (Mercier *et al.*, 2013; Hilger  
506 *et al.*, 2018, 2021; Vick *et al.*, 2022), but also in Karakorum (Shroder *et al.*, 2011) or the Andes  
507 (Fauqué *et al.*, 2009). Many of these sites record re-activations or secondary clusters during the  
508 Sub-Boreal period (Hermanns and Longva, 2013).

509 In Fig. 6 we compare frequency curves of the post Younger Dryas boulders dated in the  
510 Romanian Carpathians and of the RSF ages compiled from these studies after excluding the  
511 mountain ranges which are influenced by excess of humidity/dryness and correspondently by  
512 their variability in time (e.g., Himalaya, Atlas or Cascade Mts). Overall, the Romanian  
513 Carpathians show a similar general trend with the other world-wide catenae but with an  
514 apparently more rapid and accentuated response to the Early Holocene warming and more  
515 humid conditions, so that almost 3/4 of the dated RSF occurred before 8 ka with the highest  
516 frequency window positioned during 11.6-9 ka. Conversely, the multi-sites curve reflects a  
517 higher sensitivity of RW (deduced via RSF occurrence) to the Holocene Climatic Optimum,  
518 which can be explained both by delays in local deglaciation momentum and topoclimatic  
519 conditions. Given the relatively small number of samples used in our study (38), this first attempt  
520 to assess the RSF evolution in the Romanian Carpathians might also be biased towards the  
521 Early Holocene by the high frequency of the high-altitude samples (71% of the samples are  
522 >1700 m). As future research, it is necessary to expand the RSF dating by including more cases  
523 from the mid and low levels and to compare their histories in order to disentangle the influence  
524 of deglaciation, permafrost thawing, thermal and humidity variation. However, some of the  
525 European studies describe some similar results with the newly-obtained in the Romanian  
526 Carpathians, such as Hermanns and Longva (2013) which give an estimation of Holocene RSF  
527 magnitude in Storfjorden, Norway, showing that the earliest events (12.5 to 10 kyrs) generated  
528 by far the largest detached volumes (Fig. 6), compared to the ones dating after 8 kyrs. Similarly,  
529 reconstructed magnitudes of large landslides from the Alps (Soldati *et al.*, 2004; Ivy-Ochs *et al.*,  
530 2009), place such events in the first millennia of the Holocene.

531 Independently of the absolute exposure ages used to assess the RSF probability occurrence  
 532 during Holocene (Fig. 6), the other four surface ages from Doamnei rock glacier, in the central  
 533 Făgăraș massif, indicate multiple phases of debris accumulation, and, in the same time, the  
 534 high magnitude of early–Holocene debris production, which supplied at least the lower half of  
 535 the rock glacier body, demonstrated by the rapid accumulation of massive boulders as well as  
 536 their displacement between 12.97 and 9.91 ka ago. RW permafrost decay would have further  
 537 enhanced subsequent rockfall or rock avalanches of smaller magnitude during the following  
 538 warm episodes of the Holocene as also described in the Swiss Alps by Nagelisen *et al.*, (2015).  
 539 The particularly large boulders in the lower half of Doamnei rock glacier are incompatible with  
 540 frost-cracking intensities estimated for the Holocene (Savi et al., 2015) and were most probably  
 541 produced by similar high magnitude (as described by Hermanns and Longva, 2013) slope  
 542 failures induced by slope relaxation, permafrost degradation and overall weakened slope  
 543 coherence. We consider this to be the ultimate process/interval of intense modelling in the  
 544 alpine area of the Carpathians which defined the rock walls – rock glaciers/debris systems  
 545 preserved until present.



547 **Figure 6** Cumulated distribution of surface exposure ages attributed to post-Younger Dryas RSF in the Romanian  
548 Carpathians (blue line), and multi-site composed RSF distribution (red line) using absolute ages from the French Alps  
549 (Cossart *et al.*, 2008), Swiss Alps (Ivy-Ochs *et al.*, 2009), Italian Alps (Hormes *et al.*, 2008), Central Andes (Fauque *et*  
550 *al.*, 2009), Northern Iceland (Mercier *et al.*, 2013), Central Karakoram (Shroder *et al.*, 2011), Scotland and NW Ireland  
551 (Ballantyne *et al.*, 2014). Grey-filled columns represent estimated volume of Holocene RSF in Norway (after  
552 Hermanns and Longva, 2013)

553

## 554 **6. CONCLUSIONS**

555 The distribution of RW mapped in the Southern and Eastern Carpathians depends mainly on the  
556 lithology, structure but also weathering processes. In the metamorphic and igneous units, it  
557 ultimately relates to geomorphological context, being mostly associated with glacial cirques and  
558 valleys headwalls. Most RW are therefore restricted to the highest ridge sectors, while their low  
559 heights and areas are explained as a consequence of the lithological predisposition to debris  
560 production, especially in permafrost degrading conditions during warming phases of the Early  
561 Holocene. The North/South asymmetry in rock glaciers distribution (also signalled in other mid-  
562 latitude ranges) is reflected by the lack of South-exposed RW. We assume more stable  
563 conditions prone to fine debris and soil formation on the southern slopes due to insolation and  
564 warmer conditions.

565 For the sedimentary RW, tectonics and the geological structure are the main controls to explain  
566 the occurrence of the large (wide and high) limestone and conglomerate RW in the Romanian  
567 Carpathians. Except for Bucegi Mts, which were high and large enough to host complex glaciers  
568 during the last glaciation, most of the sedimentary units from SC and EC were not subject to  
569 glacial erosion during LGM due to either steep topography (e.g., hogback ridges) or lower  
570 altitude, although RW permafrost was probably widespread.

571 Absolute exposure ages confirm that an intense rock slope degradation via rock-slope failures  
572 took place in the Carpathian metamorphic and igneous units in Early Holocene, similar with  
573 other European sites, reaching the highest magnitudes 11.6 – 9 ka ago especially above 1800

574 m altitude. We associate the present distribution of RW with this periglacially-active period  
575 which was the last time of rock surfaces substantial reshape.

576

577 **Acknowledgements:** The research financing these results received funding from the Norway  
578 Grants 2014-2021 (project code RO-NO-2019-0415 / contract no. 30/2020), from University of  
579 Bucharest grants (project code C1.2.PFE-CDI.2021-587) and from the Research Institute of the  
580 University of Bucharest fellowship for young researchers (2018-2019 grants, awarded to MV).

581

## 582 **References**

583 Allen, S. and Huggel, C. (2013) 'Extremely warm temperatures as a potential cause of recent high mountain rockfall', *Global and*  
584 *Planetary Change*, 107, pp. 59–69. doi: 10.1016/j.gloplacha.2013.04.007.

585 Ardelean, A. C. *et al.* (2017) 'Quantifying postglacial sediment storage and denudation rates in a small alpine catchment of the  
586 Făgăraş Mountains (Romania)', *Science of the Total Environment*, 599–600 (March 2018), pp. 1756–1767. doi:  
587 10.1016/j.scitotenv.2017.05.131.

588 Ardelean, F. (2013) *Clasificarea semi-automată a unor forme de relief pentru cartarea geomorfologică. Studiu de caz Munții Țarcu.*  
589 West University of Timișoara.

590 Ardelean, F., Török-Oance, M. and Drăguț, L. (2012) 'Object-based detection of planation surfaces from Digital Elevation Models.  
591 Case study Țarcu Mountains, Southern Carpathians, Romania', in *Forum Carpathicum, From data to knowledge, from knowledge to*  
592 *action.*, pp. 127–128.

593 Bădescu, B. and Tîrlă, L. (2020) *Harta carstului din România, 2020.* Exploratorii, Asociația speologică.

594 Balco, G. *et al.* (2008) 'A complete and easily accessible means of calculating surface exposure ages or erosion rates from 10 Be  
595 and 26 Al measurements', 3, pp. 174–195. doi: 10.1016/j.quageo.2007.12.001.

596 Ballantyne, C. K. *et al.* (2014) 'Enhanced rock-slope failure following ice-sheet deglaciation: Timing and causes', *Earth Surface*  
597 *Processes and Landforms*, 39(7), pp. 900–913. doi: 10.1002/esp.3495.

598 Baroni, C., Carton, A. and Seppi, R. (2004) 'Distribution and behaviour of rock glaciers in the Adamello-Presanella massif (Italian  
599 Alps)', *Permafrost and Periglacial Processes*, 15(3), pp. 243–259. doi: 10.1002/ppp.497.

600 Bartosch, T., Stüwe, K. and Robl, J. (2017) 'Topographic evolution of the Eastern Alps: The influence of strike-slip faulting activity',  
601 *Lithosphere*, 9(3), pp. 384–398. doi: 10.1130/L594.1.

602 Borchers, B. *et al.* (2016) 'Geological calibration of spallation production rates in the CRONUS-Earth project', *Quaternary*  
603 *Geochronology*, 31, pp. 188–198. doi: 10.1016/j.quageo.2015.01.009.

604 Braucher, R. *et al.* (2003) 'In situ produced 10Be measurements at great depths: implications for production rates by fast muons',  
605 *Earth and Planetary Science Letters*, 211(3–4), pp. 251–258. doi: 10.1016/S0012-821X(03)00205-X.

606 Braucher, R. *et al.* (2011) 'Production of cosmogenic radionuclides at great depth: A multi element approach'. doi:  
607 10.1016/j.epsl.2011.06.036.

608 Braucher, R. *et al.* (2015) 'Preparation of ASTER in-house  $^{10}\text{Be}/^{9}\text{Be}$  standard solutions', *Nuclear Instruments and Methods in*  
609 *Physics Research Section B: Beam Interactions with Materials and Atoms*, 361, pp. 335–340. doi: 10.1016/J.NIMB.2015.06.012.

610 Chmeleff, J. *et al.* (2010) 'Determination of the  $^{10}\text{Be}$  half-life by multicollector ICP-MS and liquid scintillation counting', *Nuclear*  
611 *Instruments and Methods in Physics Research, Section B: Beam Interactions with Materials and Atoms*, 268(2), pp. 192–199. doi:  
612 10.1016/j.nimb.2009.09.012.

613 Corona, C., Trappmann, D. and Stoffel, M. (2013) 'Parameterization of rockfall source areas and magnitudes with ecological  
614 recorders: When disturbances in trees serve the calibration and validation of simulation runs', *Geomorphology*, 202, pp. 33–42. doi:  
615 10.1016/j.geomorph.2013.02.001.

616 Cossart, E. *et al.* (2008) 'Slope instability in relation to glacial debuitressing in alpine areas (Upper Durance catchment,  
617 southeastern France): Evidence from field data and  $^{10}\text{Be}$  cosmic ray exposure ages', *Geomorphology*, 95(1–2), pp. 3–26. doi:  
618 10.1016/j.geomorph.2006.12.022.

619 Curry, A. M. and Morris, C. J. (2004) 'Lateglacial and Holocene talus slope development and rockwall retreat on Mynydd Du, UK',  
620 *Geomorphology*, 58(1–4), pp. 85–106. doi: 10.1016/S0169-555X(03)00226-5.

621 Dunn, O. J. (1961) 'Multiple Comparisons among Means', *Journal of the American Statistical Association*, 56(293), pp. 52–64. doi:  
622 10.1080/01621459.1961.10482090.

623 Egli, M. *et al.* (2010) 'The effects of exposure and climate on the weathering of late Pleistocene and Holocene Alpine soils',  
624 *Geomorphology*, 114(3), pp. 466–482. doi: 10.1016/j.geomorph.2009.08.008.

625 Ellis, M. A. and Barnes, J. B. (2015) 'A global perspective on the topographic response to fault growth', *Geosphere*, 11(4), pp. 1008–  
626 1023. doi: 10.1130/GES01156.1.

627 Eppes, M. C. *et al.* (2016) 'Deciphering the role of solar-induced thermal stresses in rock weathering', *Bulletin of the Geological*  
628 *Society of America*, 128(9–10), pp. 1315–1338. doi: 10.1130/B31422.1.

629 Gheorghiu, D. M. (2012) 'Testing climate synchronicity between Scotland and Romania since the last glacial maximum', pp. 1–214.  
630 Available at: <http://theses.gla.ac.uk/3362/>.

631 Gheorghiu, D. M. *et al.* (2015) 'Deglaciation constraints in the Parâng Mountains, Southern Romania, using surface exposure  
632 dating', *Quaternary International*, 388(March 2016), pp. 156–167. doi: 10.1016/j.quaint.2015.04.059.

633 Girard, L. *et al.* (2013) 'Environmental controls of frost cracking revealed through in situ acoustic emission measurements in steep  
634 bedrock', *Geophysical Research Letters*, 40(9), pp. 1748–1753. doi: 10.1002/grl.50384.

635 Gruber, S. (2007) 'A mass-conserving fast algorithm to parameterize gravitational transport and deposition using digital elevation  
636 models', 43, pp. 1–8. doi: 10.1029/2006WR004868.

637 Gruber, S., Hoelzle, M. and Haerberli, W. (2004) 'Permafrost thaw and destabilization of Alpine rock walls in the hot summer of  
638 2003', *Geophysical Research Letters*, 31(13), pp. 1–4. doi: 10.1029/2004GL020051.

639 Hales, T. C. and Roering, J. J. (2007) 'Climatic controls on frost cracking and implications for the evolution of bedrock landscapes',  
640 *Journal of Geophysical Research: Earth Surface*, 112(2), pp. 1–14. doi: 10.1029/2006JF000616.

641 Hermanns, R. L. and Hewitt, K. (2009) 'Aconcagua y su relación con depósitos asignados', (June 2014).

642 Hermanns, R. L. and Longva, O. (2013) 'Rapid rock-slope failures', *Landslides*, (January), pp. 59–70. doi:  
643 10.1017/cbo9780511740367.007.

644 Hilger, P. *et al.* (2018) 'Multiple rock-slope failures from Mannen in Romsdal Valley, western Norway, revealed from Quaternary  
645 geological mapping and <sup>10</sup>Be exposure dating', *Holocene*, 28(12), pp. 1841–1854. doi: 10.1177/0959683618798165.

646 Hilger, P. *et al.* (2021) 'Permafrost as a first order control on long-term rock-slope deformation in (Sub-)Arctic Norway', *Quaternary  
647 Science Reviews*, 251, p. 106718. doi: 10.1016/j.quascirev.2020.106718.

648 Hoeven, A. G. A. Van Der *et al.* (2005) 'Observation of present-day tectonic motions in the Southeastern Carpathians: Results of the  
649 ISES / CRC-461 GPS measurements', 239, pp. 177–184. doi: 10.1016/j.epsl.2005.09.018.

650 Hormes, A. *et al.* (2008) '<sup>10</sup>Be exposure ages of a rock avalanche and a late glacial moraine in Alta Valtellina, Italian Alps',  
651 *Quaternary International*, 190(1), pp. 136–145. doi: 10.1016/j.quaint.2007.06.036.

652 Huggett, R. J. (2007) *Fundamentals of Geomorphology*. Routledge.

653 Hughes, P. D., Gibbard, P. L. and Woodward, J. C. (2007) 'Geological controls on Pleistocene glaciation and cirque form in Greece',  
654 *Geomorphology*, 88(3–4), pp. 242–253. doi: 10.1016/j.geomorph.2006.11.008.

655 Iancu, S. (1970) *Masivul Parâng. Studiu Geomorfologic*. University of Bucharest.

656 Ivy-Ochs, S. *et al.* (2009) 'Surface exposure dating of the Flims landslide, Graubünden, Switzerland', *Geomorphology*, 103(1), pp.  
657 104–112. doi: 10.1016/j.geomorph.2007.10.024.

658 Johnson, B. G., Thackray, G. D. and Van Kirk, R. (2007) 'The effect of topography, latitude, and lithology on rock glacier distribution  
659 in the Lemhi Range, central Idaho, USA', *Geomorphology*, 91(1–2), pp. 38–50. doi: 10.1016/j.geomorph.2007.01.023.

660 Krautblatter, M., Funk, D. and Günzel, F. K. (2013) 'Why permafrost rocks become unstable: A rock-ice-mechanical model in time  
661 and space', *Earth Surface Processes and Landforms*, 38(8), pp. 876–887. doi: 10.1002/esp.3374.

662 Kromer, R. (2017) 'Identifying and Monitoring Rockfall Precursors Using Terrestrial Laser Scanning for Improved Rockfall Hazard  
663 Management', p. 313. Available at: <https://qspace.library.queensu.ca/handle/1974/22765>.

664 Kruskal, W. H. and Wallis, W. A. (1952) 'Use of Ranks in One-Criterion Variance Analysis', *Journal of the American Statistical  
665 Association*, 47(260), p. 583. doi: 10.2307/2280779.

666 Lifton, Z. M. *et al.* (2009) 'Influence of rock strength on the valley morphometry of Big Creek, central Idaho, USA', *Geomorphology*,  
667 111(3–4), pp. 173–181. doi: 10.1016/j.geomorph.2009.04.014.

668 Linzer, H. G. *et al.* (1998) 'Kinematic evolution of the Romanian Carpathians', *Tectonophysics*, 297(1–4), pp. 133–156. doi:  
669 10.1016/S0040-1951(98)00166-8.

670 Loyer, A., Jaboyedoff, M. and Pedrazzini, A. (2009) 'Identification of potential rockfall source areas at a regional scale using a DEM-  
671 based geomorphometric analysis', *Natural Hazards and Earth System Science*, 9(5), pp. 1643–1653. doi: 10.5194/nhess-9-1643-  
672 2009.

673 Magnin, F. *et al.* (2015) 'Determination of warm, sensitive permafrost areas in near-vertical rockwalls and evaluation of distributed  
674 models by electrical resistivity tomography', *Journal of Geophysical Research: Earth Surface*, 120(5), pp. 745–762. doi:  
675 10.1002/2014JF003351.

676 Matsuoka, N. (2008) 'Frost weathering and rockwall erosion in the southeastern Swiss Alps: Long-term (1994-2006) observations',  
677 *Geomorphology*, 99(1–4), pp. 353–368. doi: 10.1016/j.geomorph.2007.11.013.

678 Matthews, J. A. *et al.* (2018) 'Small rock-slope failures conditioned by Holocene permafrost degradation: a new approach and  
679 conceptual model based on Schmidt-hammer exposure-age dating, Jotunheimen, southern Norway', *Boreas*, 47(4), pp. 1144–1169.  
680 doi: 10.1111/bor.12336.

681 McKight, P. E. and Najab, J. (2010) 'Kruskal-Wallis Test', *The Corsini Encyclopedia of Psychology*, pp. 1–1. doi:  
682 10.1002/9780470479216.CORPSY0491.

683 Merchel, S. *et al.* (2008) 'Towards more precise  $^{10}\text{Be}$  and  $^{36}\text{Cl}$  data from measurements at the  $10\text{ \AA}^{14}$  level: Influence of sample  
684 preparation', *Nuclear Inst. and Methods in Physics Research, B*, 266, pp. 4921–4926. doi: 10.1016/j.nimb.2008.07.031.

685 Merchel, S. and Herpers, U. (1999) 'An update on radiochemical separation techniques for the determination of long-lived  
686 radionuclides via accelerator mass spectrometry', *Radiochimica Acta*, 84, pp. 215–219.

687 Mercier, D. *et al.* (2013) 'The Höfðáahólar rock avalanche (sturzström): Chronological constraint of paraglacial landsliding on an  
688 Icelandic hillslope', *Holocene*, 23(3), pp. 432–446. doi: 10.1177/0959683612463104.

689 Merten, S. (2011) *Thermo-tectonic evolution of a convergent orogen with low topographic build-up: Exhumation and kinematic  
690 patterns in the Romanian Carpathians derived from thermochronology*. Vrije Universiteit Amsterdam. Available at:  
691 <https://research.vu.nl/en/publications/thermo-tectonic-evolution-of-a-convergent-orogen-with-low-topogra>.

692 Messenzehl, K. *et al.* (2017) 'Regional-scale controls on the spatial activity of rockfalls (Turtmann Valley, Swiss Alps) — A  
693 multivariate modeling approach', *Geomorphology*, 287, pp. 29–45. doi: 10.1016/j.geomorph.2016.01.008.

694 Micu, D. M. *et al.* (2015) *Climate of the Romanian Carpathians*. doi: 10.1007/978-3-319-02886-6.

695 Mîndrescu, M. (2016) *Geomorfometria circurilor glaciare din Carpații românești*. Editura Universității din Suceava.

696 Mîndrescu, M., Cristea, I. A. and Hutchinson, S. M. (2010) 'Bathymetric and sedimentological changes of glacial lake Știol, Rodna  
697 Masiff, *Carpathian Journal of Earth and Environmental Sciences*, 5(1), pp. 57–65.

698 Mîndrescu, M. and Evans, I. S. (2014) 'Cirque form and development in Romania: Allometry and the buzzsaw hypothesis',  
699 *Geomorphology*, 208, pp. 117–136. doi: 10.1016/j.geomorph.2013.11.019.

700 Mîndrescu, M., Evans, I. S. and Cox, N. J. (2010) 'Climatic implications of cirque distribution in the Romanian Carpathians:  
701 Palaeowind directions during glacial periods', *Journal of Quaternary Science*, 25(6), pp. 875–888. doi: 10.1002/jqs.1363.

702 Mutihac, V. (1990) *Structura geologică a teritoriului României*. Editura Tehnică.

703 Mutihac, V. (2004) *Gologia României*. București: Editura Didactică și Pedagogică.

704 Nagelisen, J. *et al.* (2015) 'Post-glacial rock avalanches in the Obersee Valley, Glarner Alps, Switzerland', *Geomorphology*, 238, pp.  
705 94–111. doi: 10.1016/j.geomorph.2015.02.031.

706 Onaca, A. *et al.* (2013) 'Assesment of internal structure of periglacial landforms from southern carpathians (Romania) using dc  
707 resistivity tomography', *Carpathian Journal of Earth and Environmental Sciences*, 8(2), pp. 113–122.

708 Onaca, A. *et al.* (2015) 'Near surface thermal characteristics of alpine steep rockwalls in the Retezat Mountains', *Forum geografic*,  
709 XIV(2), pp. 124–133. doi: 10.5775/fg.2067-4635.2015.091.d.

710 Onaca, A., Urdea, P., *et al.* (2017) 'Present-Day Periglacial Processes in the Alpine Zone', in Rădoane, M. and Vespremeanu-Stroe,

711 A. (eds) *Landforms dynamics and evolution in Romania*. Springer International Publishing, pp. 147–176. doi: 10.1007/978-3-319-  
712 32589-7\_7.

713 Onaca, A., Ardelean, F., et al. (2017) 'Southern Carpathian rock glaciers: Inventory, distribution and environmental controlling  
714 factors', *Geomorphology*, 293, pp. 391–404. doi: 10.1016/j.geomorph.2016.03.032.

715 Pánek, T. et al. (2016) 'Cosmogenic age constraints on post-LGM catastrophic rock slope failures in the Tatra Mountains (Western  
716 Carpathians)', *Catena*, 138(March), pp. 52–67. doi: 10.1016/j.catena.2015.11.005.

717 Phillips, M. et al. (2017) 'Rock slope failure in a recently deglaciated permafrost rock wall at Piz Kesch (Eastern Swiss Alps),  
718 February 2014', *Earth Surface Processes and Landforms*, 42(3), pp. 426–438. doi: 10.1002/esp.3992.

719 Popescu, R. et al. (2017) 'Spatial Distribution and Main Characteristics of Alpine Permafrost from Southern Carpathians, Romania',  
720 in Rădoane, M. and Vespremeanu-Stroe, A. (eds) *Landforms dynamics and evolution in Romania*. Springer International Publishing,  
721 pp. 117–146. doi: 10.1007/978-3-319-32589-7\_6.

722 Popescu, R., Urdea, P. and Vespremeanu-Stroe, A. (2017) 'Deglaciation History of High Massifs from the Romanian Carpathians:  
723 Towards an Integrated View', in *Landforms dynamics and evolution in Romania*. Springer International Publishing, pp. 87–117. doi:  
724 10.1007/978-3-319-32589-7\_5.

725 Povară, I. et al. (2013) 'Water flow system within the Cerna Valley graben structure (SW of the Southern Carpathians, Romania)', in  
726 *International Symposium on Hierarchical Flow Systems in Karst Regions*.

727 Prager, C. et al. (2008) 'Age distribution of fossil landslides in the Tyrol (Austria) and its surrounding areas', *Natural Hazards and  
728 Earth System Science*, 8(2), pp. 377–407. doi: 10.5194/nhess-8-377-2008.

729 Reuther, A. U. et al. (2007) 'Late Pleistocene glacial chronology of the Pietrele Valley, Retezat Mountains, Southern Carpathians  
730 constrained by  $^{10}\text{Be}$  exposure ages and pedological investigations', *Quaternary International*, 164–165, pp. 151–169. doi:  
731 10.1016/j.quaint.2006.10.011.

732 Rode, M., Schnepfleitner, H. and Sass, O. (2016) 'Simulation of moisture content in alpine rockwalls during freeze–thaw events',  
733 *Earth Surface Processes and Landforms*, 41(13), pp. 1937–1950. doi: 10.1002/esp.3961.

734 Ruszkiczay-Rüdiger, Z. et al. (2021) 'Limited glacial erosion during the last glaciation in mid-latitude cirques (Retezat Mts, Southern  
735 Carpathians, Romania)', *Geomorphology*, 384, p. 107719. doi: 10.1016/j.geomorph.2021.107719.

736 Săndulescu, M. (1984) *Geotectonica României*. Editura Tehnică.

737 Sauchyn, D. J., Cruden, D. M. and Hu, X. Q. (1998) 'Structural control of the morphometry of open rock basins, Kananaskis region,  
738 Canadian Rocky Mountains', *Geomorphology*, 22(3–4), pp. 313–324. doi: 10.1016/S0169-555X(97)00083-4.

739 Savi, S., Delunel, R. and Schlunegger, F. (2015) 'Efficiency of frost-cracking processes through space and time: An example from  
740 the eastern Italian Alps', *Geomorphology*, 232, pp. 248–260. doi: 10.1016/j.geomorph.2015.01.009.

741 Seong, Y. B. et al. (2009) 'Rates of basin-wide rockwall retreat in the K2 region of the Central Karakoram defined by terrestrial  
742 cosmogenic nuclide  $^{10}\text{Be}$ ', *Geomorphology*, 107(3–4), pp. 254–262. doi: 10.1016/j.geomorph.2008.12.014.

743 Shapiro, S. S. and Wilk, M. B. (1965) 'An Analysis of Variance Test for Normality (Complete Samples)', *Biometrika*, 52(3/4), p. 591.  
744 doi: 10.2307/2333709.

745 Shroder, J. F. et al. (2011) 'The role of mass movements on landscape evolution in the Central Karakoram: Discussion and

746 speculation', *Quaternary International*, 236(1–2), pp. 34–47. doi: 10.1016/j.quaint.2010.05.024.

747 Soldati, M., Corsini, A. and Pasuto, A. (2004) 'Landslides and climate change in the Italian Dolomites since the Late glacial', *Catena*,

748 55(2), pp. 141–161. doi: 10.1016/S0341-8162(03)00113-9.

749 Stone, J. O. (2000) 'Air pressure and cosmogenic isotope production', *Journal of Geophysical Research: Solid Earth*, 105(B10), pp.

750 23753–23759. doi: 10.1029/2000JB900181.

751 Tămaş, T., Onac, B. P. and Bojar, A. V. (2005) 'Lateglacial-Middle Holocene stable isotope records in two coeval stalagmites from

752 the Bihor Mountains, NW Romania', *Geological Quarterly*, 49(2), pp. 185–194.

753 Török-Oance, M. and Ardelean, F. (2012) 'Object-oriented image analysis for detection of the barren karst areas. A case study: the

754 central sector of the Mehedinţi Mountains (Southern Carpathians)', *Carpathian Journal of Earth and Environmental Sciences*, 7, pp.

755 248–254.

756 Urdea, P. (2000) *Munţii Retezat. Studiu Geomorfologic*. Bucureşti: Editura Academiei Române.

757 Vaida, M. and Verniers, J. (2005) 'Biostratigraphy and palaeogeography of lower Devonian chitinozoans, from east and west

758 Moesia, Romania', *Geologica Belgica*, 8(4), pp. 121–130.

759 Vasile, M. and Vespremeanu-Stroe, A. (2017) *Thermal weathering and distribution of mountain Rockwalls*, *Springer Geography*. doi:

760 10.1007/978-3-319-32589-7\_8.

761 Vasile, Mirela and Vespremeanu-Stroe, A. (2017) 'Thermal Weathering and Distribution of Mountain Rockwalls', in Rădoane, M. and

762 Vespremeanu-Stroe, A. (eds) *Landforms dynamics and evolution in Romania*. Springer International Publishing, pp. 177–196. doi:

763 10.1007/978-3-319-32589-7\_8.

764 Vermeesch, P. (2007) 'CosmoCalc: An Excel add-in for cosmogenic nuclide calculations', *Geochemistry, Geophysics, Geosystems*,

765 8(8), p. 8003. doi: 10.1029/2006GC001530.

766 Vespremeanu-Stroe, A., Cheval, S. and Tătui, F. (2012) 'The wind regime of Romania – Characteristics, trends and North Atlantic

767 oscillation influences', *Forum geografic*, XI(2), pp. 118–126. doi: 10.5775/fg.2067-4635.2012.003.d.

768 Vick, L. M. *et al.* (2022) 'Evolution and temporal constraints of a multiphase postglacial rock slope failure', *Geomorphology*, 398. doi:

769 10.1016/j.geomorph.2021.108069.

770 Willett, S. D. (1999) 'Orogeny and orography: The effects of erosion on the structure of mountain belts', *Journal of Geophysical*

771 *Research: Solid Earth*, 104(B12), pp. 28957–28981. doi: 10.1029/1999jb900248.